atmosphere

MDPI

Review

Hydrogenation of Carbon Dioxide to Value-Added Liquid Fuels and Aromatics over Fe-Based Catalysts Based on the Fischer–Tropsch Synthesis Route

Qiang Wang [1,†], Kehao Hu [1,†], Ruxing Gao [2,*], Leiyu Zhang [1], Lei Wang [2] and Chundong Zhang [1,*]

[1] State Key Laboratory of Materials-Oriented Chemical Engineering, College of Chemical Engineering, Nanjing Tech University, Nanjing 211816, China
[2] School of Energy Science and Engineering, Nanjing Tech University, Nanjing 211816, China
* Correspondence: grxing@njtech.edu.cn (R.G.); zhangcd@njtech.edu.cn (C.Z.)
† These authors contributed equally to this work.

Abstract: Hydrogenation of CO_2 to value-added chemicals and fuels not only effectively alleviates climate change but also reduces over-dependence on fossil fuels. Therefore, much attention has been paid to the chemical conversion of CO_2 to value-added products, such as liquid fuels and aromatics. Recently, efficient catalysts have been developed to face the challenge of the chemical inertness of CO_2 and the difficulty of C–C coupling. Considering the lack of a detailed summary on hydrogenation of CO_2 to liquid fuels and aromatics via the Fischer–Tropsch synthesis (FTS) route, we conducted a comprehensive and systematic review of the research progress on the development of efficient catalysts for hydrogenation of CO_2 to liquid fuels and aromatics. In this work, we summarized the factors influencing the catalytic activity and stability of various catalysts, the strategies for optimizing catalytic performance and product distribution, the effects of reaction conditions on catalytic performance, and possible reaction mechanisms for CO_2 hydrogenation via the FTS route. Furthermore, we also provided an overview of the challenges and opportunities for future research associated with hydrogenation of CO_2 to liquid fuels and aromatics.

Keywords: CO_2 hydrogenation; liquid fuels; aromatics; Fischer–Tropsch synthesis; Fe-based catalysts; HZSM-5

check for updates

Citation: Wang, Q.; Hu, K.; Gao, R.; Zhang, L.; Wang, L.; Zhang, C. Hydrogenation of Carbon Dioxide to Value-Added Liquid Fuels and Aromatics over Fe-Based Catalysts Based on the Fischer–Tropsch Synthesis Route. *Atmosphere* **2022**, *13*, 1238. https://doi.org/10.3390/atmos13081238

Academic Editor: Marcelo I. Guzman

Received: 6 June 2022
Accepted: 2 August 2022
Published: 4 August 2022

1. Introduction

With the rapid growth of the world's population and the development of the industrial sectors, fossil fuels have made important contributions to economic and social development. However, the overuse of fossil fuels has resulted in large amounts of CO_2 emissions and a series of environmental problems, such as global warming, natural disasters, extreme weather, etc. [1–3]. In order to reduce CO_2 emissions and to achieve carbon neutrality, it is necessary to adopt low-carbon renewable energy (such as wind and solar energy) and to develop efficient CO_2 capture and utilization (CCU) technologies [4,5]. The utilization of renewable energy can effectively reduce CO_2 emissions, but it is currently difficult to be deployed on a large scale due to its characteristics of fluctuation and intermittency under changing natural conditions. By contrast, CCU technologies treat CO_2 as a renewable carbon source and convert it into high value-added chemicals and fuels, which can significantly reduce both CO_2 emissions and the dependence on fossil energy.

Among various CCU technologies, the thermocatalytic conversion of CO_2 has received widespread attention from industry and academia due to its high industrial application potential, as well as adjustable product selectivity. In addition, among the thermocatalytic conversion technologies, CO_2 hydrogenation has been the main focus and has made considerable progress in pilot-scale and large-scale applications [6–11], especially for the production of C1 molecules (CH_4 [12–15], CH_3OH [16], HCOOH [17–19], etc.). Furthermore,

long-chain hydrocarbons with higher added value (i.e., liquid fuels and aromatics) have recently received extensive attention due to their wide applications in the transportation and petrochemical industries. Herein, for liquid fuels, they are widely used as transportation fuels (e.g., gasoline, jet fuel, and diesel) and play a significant role in the global energy supply market [11]. For aromatics, they are important commodity petrochemicals and are generally identified as the important platform chemicals for the production of solvents, value-added chemicals, and polymers [20,21]. Currently, the production of liquid fuels and aromatics heavily depends on petroleum cracking and catalytic reforming, which exacerbates the depletion of fossil fuels and results in considerable CO_2 emissions. In this paper, an alternative strategy for hydrogenation of CO_2 to liquid fuels and aromatics provides a promising and sustainable route for mitigating carbon emissions and producing high value-added fuels and chemicals.

Generally, studies on the hydrogenation of CO_2 to hydrocarbons can be divided into two possible routes: Fischer–Tropsch synthesis (FTS) and methanol-mediated routes [22]. For the FTS route, CO intermediates produced from reverse water-gas-shift (RWGS) can be converted to C_{2+} hydrocarbons. Furthermore, olefins in the obtained C_{2+} hydrocarbons can be further converted into aromatics over the acid sites of zeolites via a series of oligomerization, dehydrogenation, and cyclization reactions. As for the methanol-mediated route, the formation of C_{2+} hydrocarbons and aromatics requires methanol intermediate transformation via methanol-to-hydrocarbons (MTH) and methanol-to-aromatics (MTA) routes [21,23]. However, the MTH and MTA routes generally require high temperatures of 400–500 °C [20], which result in high CO selectivity due to the endothermic character of RWGS, and this is not conducive to enhancing the yield of high value-added chemicals [24]. Therefore, the FTS route is preferred for producing long-chain hydrocarbons and aromatics via CO_2 hydrogenation. However, the production of long-chain hydrocarbons with higher added value still faces many challenges due to the high C–C coupling barrier during the CO_2 hydrogenation process. In recent years, several efficient catalysts with excellent catalytic performance have been applied to convert CO_2 to long-chain hydrocarbons. Considering the lack of reviews on current research progress on the hydrogenation of CO_2 to liquid hydrocarbons (i.e., liquid fuels and aromatics), we conducted a systematic and comprehensive summary of recent advances in the development of highly efficient catalysts for CO_2 hydrogenation. Herein, we mainly focus on the research progress regarding the synthesis of liquid fuels and aromatics via the FTS route.

This work is mainly divided into three sections: (1) Hydrogenation of CO_2 to liquid fuels over modified Fe-based catalysts or multifunctional catalysts combined with Fe-based catalytic components and zeolites. Herein, the effects of alkali promoters, secondary metals, catalyst supports, preparation methods, zeolite pre-treatments, and reaction conditions on the catalytic performance are discussed in detail. (2) Hydrogenation of CO_2 to aromatics over FeO_x/zeolite tandem catalysts, where the effects of promoters, catalyst supports, and preparation methods of Fe-based catalysts, the effects of acidic sites, the types of acidity, and the preparation methods of zeolites, and the effects of the reaction conditions on the overall catalytic performance of the tandem catalysts are illustrated. (3) Reaction mechanisms of CO_2 hydrogenation, where the possible reaction mechanisms for hydrogenation of CO_2 to liquid fuels and aromatics via the FTS route are summarized in detail. Moreover, the main contributions of this work are as follows: (1) A comprehensive and systematic review of the research progress on the development of efficient catalysts for the hydrogenation of CO_2 to liquid fuels and aromatics via the FTS route is implemented. (2) The key factors influencing the catalytic activity and stability of various catalysts and the strategies for optimizing the catalytic performance and product distribution, as well as the effects of the reaction conditions on catalytic performance are discussed in detail. (3) The possible reaction mechanisms for the hydrogenation of CO_2 into liquid fuels and aromatics via the FTS route are summarized. (4) An overview of the challenges and opportunities for future research regarding CO_2 hydrogenation to value-added products is proposed, providing very important guidelines for the preparation of highly efficient CO_2 hydrogenation catalysts.

2. Direct Hydrogenation of CO_2 to Liquid Fuels over Fe-Based Catalysts

Hydrogenation of CO_2 to liquid fuels via the FTS route (Equation (1)) usually includes two steps: First, CO_2 is converted to CO by RWGS (Equation (2)) and then CO is converted to liquid fuels by FTS (Equation (3)). Various catalysts (e.g., Fe-, Co-, and Ru-based catalysts) based on catalysts for CO hydrogenation have been developed due to their excellent selectivity towards long-chain hydrocarbons [25–29]. Among them, Ru-based catalysts [27] have the best catalytic performance, however, the high catalyst costs limit their commercial application on a large scale. Instead, Fe- and Co-based catalysts have been widely studied because of their relatively high catalytic activity and low catalyst cost [22,28–33]. Typically, Fe- and Co-based catalysts are used as the industrial CO-FTS catalysts. Compared with Fe-based catalysts, Co-based catalysts exhibit higher long-chain hydrocarbon selectivity at low temperatures (<300 °C), but they tend to produce CH_4 at high temperatures (>300 °C). Due to the fact that Co-based catalysts almost have no RWGS activity, a second component (e.g., copper) with RWGS activity is necessary for converting CO_2 to CO [11]. In contrast, Fe-based catalysts have both RWGS and FTS activity, with high CO_2 conversion and low CH_4 selectivity within a wide temperature range (300–400 °C) [34–40] for CO_2 hydrogenation [22]. Herein, the recent progress on the catalysts for the hydrogenation of CO_2 to liquid fuels is mainly introduced below, and the specific representative catalysts as well as their catalytic performances are illustrated in Tables 1 and 2.

$$\mathrm{n\ CO_2 + (3n+1)\ H_2 \rightarrow C_nH_{2n+2} + 2n\ H_2O} \qquad \Delta_R H_{573K} = -128\ \mathrm{kJ{\cdot}mol^{-1}} \tag{1}$$

$$\mathrm{CO_2 + H_2 \rightleftharpoons CO + H_2O} \qquad \Delta_R H_{573K} = +38\ \mathrm{kJ{\cdot}mol^{-1}} \tag{2}$$

$$\mathrm{n\ CO + (2n+1)\ H_2 \rightarrow C_nH_{2n+2} + n\ H_2O} \qquad \Delta_R H_{573K} = -166\ \mathrm{kJ{\cdot}mol^{-1}} \tag{3}$$

Table 1. Representative catalysts and their performance for the direct hydrogenation of CO_2 to liquid fuels.

		Reaction Conditions					Hydrocarbon Distribution (%)							
Entry	**Catalysts**	**H_2/CO_2 Ratios**	**T (°C)**	**P (MPa)**	**GHSV/mL·g^{-1}·h^{-1}**	**CO_2 conv. (%)**	**CO Sel. (%)**	**CH_4**	**C_{2-4}**	**$C_{2-4}{}^{0\,a}$**	**$C_{2-4}{}^{=\,a}$**	**C_{5+}**	**O/P [b]**	**Ref.**
						Fe-based catalyst								
1	Fe-K/alumina	2.0	400	N.A.	1900	69.9	3.9	16.7	47.6	N.A.	N.A.	35.8	N.A. [g]	[41]
2	Fe_2O_3-CT600	3.0	350	1.5	1140	40	15	14.1	43.5	N.A.	N.A.	42.4	N.A.	[42]
3	Fe_5C_2-10K/a-Al_2O_3	3.0	320	3.0	3600	31.5	18.6	14.9	49.4	5.4	44.0	35.7	8.1	[16]
4	92.6Fe7.4K	3.0	300	2.5	560	41.7	6.0	11.0	29.6	6.6	23.0	59.6	3.5	[43]
5	K-Fe/ZrO_2	3.0	300	2.0	1200	43.0	15.0	18.0	53.2	N.A.	N.A.	27.8	N.A.	[44]
6	FeK/Al_2O_3	3.0	400	3.0	3600	42.5	23.9	30.0	40.5	N.A.	N.A.	29.6	N.A.	[45]
7	Fe-Cu-K-La/TiO_2	3.0	300	1.1	3600	23.2	33.0	19.4	37.3	N.A.	N.A.	43.3 [c]	N.A.	[46]
8	Fe-Cu-Al-K	3.0	265	1.3	2240 [f]	15.6	22.8	12.8	36.0	N.A.	N.A.	51.0	N.A.	[47]
9	Fe-Cu-K-Al	3.0	300	2.5	5000	35.7	N.A.	N.A.	N.A.	N.A.	N.A.	50.7	N.A.	[48]
10	$FeAlO_x$-5	3.0	330	3.5	4000	36.8	7.2	12.1	30.1	N.A.	N.A.	57.8	0.7 [h]	[49]
11	10Fe3Cu1K/Al_2O_3	3.0	400	3.0	3600	41.7	26.5	37.8	43.4	N.A.	N.A.	17.8	N.A.	[50]
12	Fe0.17Cu1K/Al_2O_3	3.0	300	1.1	3600	29.3	17.0	8.4	26.5	N.A.	N.A.	65.1	N.A.	[51]
13	$CuFeO_2$-6 [e]	3.0	300	1.0	1800	17.3	31.7	2.6	31.0	N.A.	N.A.	66.3	7.3	[52]
14	$PdKFe_2O_3$	3.0	235	1.6	6000	20.7	18.2	13.6	28.1	N.A.	N.A.	58.3	N.A.	[53]
15	FeMnNa	3.0	340	2.0	12,000	35.0	18.1	13.1	38.7	N.A.	N.A.	48.2	8.1	[54]
16	5Mn-Na/Fe	3.0	320	3.0	2040	38.6	11.7	13.4	38.8	4.5	26.6	47.8	7.5	[55]
17	Fe-Mn-K	3.0	300	1.0	2400	38.2	5.6	10.4	27.7	N.A.	N.A.	61.7	N.A.	[56]
18	$K_3/FeMn_{10}Ti_{20}$	2.8	320	5.0	24,000	34.9	9.7	9.2	27.2	12.6 [h]	N.A.	51.0	2.7	[57]
19	10Fe0.8K0.53Co	3.0	300	2.5	560	54.6	2.0	19.3	32.8	7.9	24.9	48.0	3.2	[58]
20	10Fe0.8K0.53Ru	3.0	300	2.5	560	47.1	3.1	16.9	28.0	7.6	20.3	55.1	2.7	[58]
21	Na-$ZnFe_2O_4$	3.0	340	1.0	1800	34	11.7	8.6	28.1	N.A.	N.A.	51.6	11.3	[59]
22	$ZnFe_2O_4$-nNa	3.0	320	3.0	4000	38.4	11.2	11.0	39.3	N.A.	N.A.	49.7	N.A.	[60]
23	Na-Zn-Fe	3.0	340	2.5	15,000	39.0	14.0	12.0	47.7	4.7	43.0	40.5	9.8	[40]
24	FeZn-NC	3.0	320	3.0	7200	29.3	19.9	20.7	45.1	7.6	37.5	34.2	4.9	[61]
25	FeZnK-NC	3.0	320	3.0	7200	34.6	21.2	24.2	47.7	7.1	40.6	28.0	5.7	[61]
26	N-K-600-0	3.0	400	3.0	3600	46.0	17.5	32.2	40.8	17.6	23.2	26.9	1.3	[62]
27	FeK/Co-NC	3.0	300	2.5	N.A.	51.7	21.6	N.A.	N.A.	N.A.	N.A.	42.4	N.A.	[36]
28	FeK/C-1EDA	3.0	300	1.0	N.A.	20.1	31.7	17.2	43.3	37.7	5.6	39.5	1.2	[63]
29	Fe/C-bio	3.0	320	1.0	2240 [e]	30.5	23.2	11.8	24.4	N.A.	N.A.	63.8	N.A.	[64]
30	FeK/SWNTs	3.0	340	2.0	9000	52.7	9.6	13.5	31.1	N.A.	N.A.	55.4	N.A.	[65]

Table 1. *Cont.*

Entry	Catalysts	Reaction Conditions						Hydrocarbon Distribution (%)						
		H_2/CO_2 Ratios	T (°C)	P (MPa)	GHSV/mL·g^{-1}·h^{-1}	CO_2 conv. (%)	CO Sel. (%)	CH_4	C_{2-4}	$C_{2-4}^{0\,a}$	$C_{2-4}^{=\,a}$	C_{5+}	O/P [b]	Ref.
31	Fe/CNT	2.0	350	8.5	14,400	22.0	18.0	42.7	42.7	N.A.	N.A.	14.6	N.A.	[66]
32	Na-Fe/CNTs	3.0	370	1.5	1200	48.0	24.8	27.5	52.5	N.A.	N.A.	19.9	N.A.	[67]
33	FeK/MPC	3.0	300	2.5	2000	50.6	8.2	16.8	34.7	N.A.	N.A.	48.5	N.A.	[68]
Non Fe-based catalyst														
1	Na-CoCu/TiO_2	3.0	250	5.0	3000	18.4	30.2	26.1	31.8	N.A.	N.A.	42.1	N.A.	[30]
2	2.5K-CoCu/TiO_2	3.0	250	5.0	3000	13.0	35.1	34.1	30.8	N.A.	N.A.	35.1	0.3	[31]
3	10%Co/MIL-53(Al)	3.0	260	3.0	1000	25.3	26.6	35.1	29.8	N.A.	N.A.	35.0	N.A.	[32]
4	Co_6/MnO_x	1.0	200	8.0	N.A.	15.3	0.4	N.A.	46.6 [d]	N.A.	N.A.	53.4	N.A.	[33]
5	CMO-10	3.0	270	4.0	4000	64.3	0.2	44.2	22.9	N.A.	N.A.	32.9	N.A.	[29]
6	Co-Fe-0.81Na	3.0	240	3.0	5500	10.2	5.2	17.8	9.4	N.A.	N.A.	72.9	N.A.	[28]

[a] Meaning paraffins(o) and olefins (=) in C_2–C_4, respectively, [b] Olefins/paraffins ratio of C_2-C_4 products, [c] Including a small amount of alcohol, [d] C_1-C_4, [e] Containing 0.03% sodium by mass fraction, [f] Gas volume was calculated based on the ideal gas law, [g] N.A.: Not available, [h] Oxy = oxygen compounds (MeOH + Me_2O).

Table 2. Representative catalysts and their performance for direct hydrogenation of CO_2 to iso-paraffins.

Entry	Catalysts	Reaction Conditions						Hydrocarbon Distribution (%)					
		H_2/CO_2 Ratios	T (°C)	P (MPa)	GHSV/ mL·g^{-1}·h^{-1}	CO_2 Conv. (%)	CO Select. (%)	Oxy [c]	CH_4	C_{2-4}	C_{5+}		Ref.
Multifunctional Fe-based catalyst with zeolite													
1	$FeAlO_x$-5/HZSM-5	3.0	330	3.5	4000	36.8	16.0	N.A.	10.0	20.0	70.0	N.A.	[49]
2	Na-Fe_3O_4/HZSM-5	3.0	320	3.0	4000	22.0	20.1	N.A.	4.0	16.6	79.4 [a]	N.A.	[69]
3	Na-Fe_3O_4/HZSM-5(160)	3.0	320	3.0	4000	33.6	14.2	N.A.	7.9	18.4	73.7 [b]	N.A.	[69]
4	92.6Fe7.4K/HZSM-5	3.0	300	2.5	560	43.9	6.1	N.A.	9.5	10.8 [d]	N.A.	I-C_{4-6}/C_{4-6} 69.7	[43]
5	NaFe+SAPO-11+ZSM-5	3.0	350	3.0	4800	31.2	13.20	0.7	9.2	18.3	72.5	I-C_{5+}/C_{5+} 38.2	[70]
6	K-Fe/C-KZSM-5	2.5	320	2.0	4800	34.5	18.8	N.A.	11.0	18.9	70.1	N.A.	[71]

[a] The C_{5+} products cover 78.3% of C_5–C_{11} and 1.1% of C_{12+} hydrocarbons, [b] The C_{5+} products cover 62.6% of C_5–C_{11} and 0.6% of C_{12+} hydrocarbons, [c] Oxy = oxygen compounds (MeOH + Me_2O), [d] C_2-C_3.

2.1. Strategies for Improving the Catalytic Performance of Fe-Based Catalysts

Generally, in the hydrogenation of CO_2 to liquid fuels based on Fe-based catalysts, Fe_3O_4, as the active site for RWGS, is responsible for generating CO intermediates, and iron carbides (Fe_xC_y), as the active sites for FTS, play a key role in carbon chain growth [16,72]. However, pure Fe-based catalysts usually show low CO_2 conversion and high CH_4 selectivity [73,74]. To address this issue, several strategies such as the addition of alkali promoters and secondary metals, the selection of suitable catalyst supports, and the optimization of catalyst preparation methods have been widely investigated to further enhance CO_2 conversion and to improve the selectivity towards long-chain hydrocarbons, which will be summarized below in detail.

2.1.1. Alkali Promoters

The addition of alkali promoters (K, Na, Rb, Cs, etc.) is an effective approach to enhance CO_2 conversion as well as long-chain hydrocarbon selectivity [41,44,47,48,50,56,61,62,75]. More specifically, alkali promoters can transfer electrons to the active Fe species, therefore increasing the local electron density around Fe species, which contributes to enhancing Fe–C bonds and weakening C=O bonds [76,77], thus facilitating the formation of iron carbides as well as the carbon chain growth [44]. In addition, alkali promoters can enhance CO_2 adsorption while inhibiting H_2 adsorption on the catalyst surface, which leads to a high C/H ratio and favors C–C coupling [41,78]. However, there is an optimum loading amount of alkali promoters, considering the catalytic activity, selectivity, and stability [34,36,53,79]. As shown in Figure 1, low K (a: 0→5 wt%, b: K/Fe = 0→0.3) significantly facilitates CO_2 conversion and C_{5+} hydrocarbon selectivity, accompanied by low CH_4 selectivity. However, further addition of K (a: 5→15 wt%; b: K/Fe = 0.3→1) results in an increase in CO selectivity and also suppresses selectivity towards long-chain hydrocarbons. It is because, on the one hand, excess K covers Fe active sites, which reduces CO_2 adsorption and its subsequent conversion [16]; on the other hand, excess K further enhances Fe–C bonds, which may cause severe carbon deposition due to the difficultly in C desorption [34,36], thus reducing the catalyst stability [80,81].

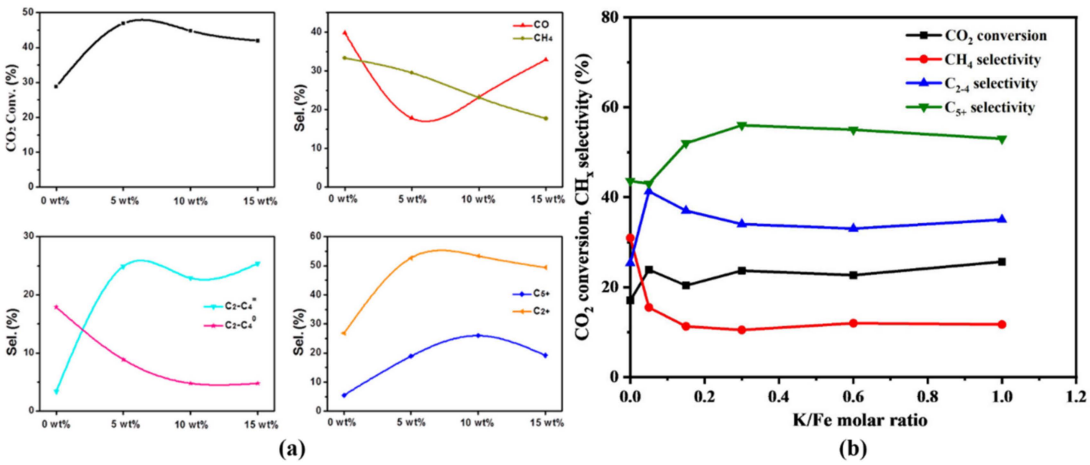

Figure 1. (**a**) Effects of the K content on the catalytic performance over Fe_5C_2-(x)K/a-Al_2O_3 catalysts. Reaction conditions: 400 °C, 3.0 MPa, GHSV = 3600 mL·g_{cat}^{-1}·h^{-1}, H_2/CO_2 = 3. Reprinted with permission from Liu et al. [16]. Copyright (2018) American Chemical Society. (**b**) Effects of the K/Fe molar ratio on the activity of the Fe-(x)K/CNT catalysts for CO_2 hydrogenation. Reaction conditions: 300 °C, 2.0 MPa, GHSV = 4000 mL·g_{cat}^{-1}·h^{-1}, H_2/CO_2 = 3. Reprinted with permission from Dai et al. [82]. Copyright (2021) WILEY.

2.1.2. Secondary Metals

The addition of secondary metals (Cu, Co, Zn, etc.) is another reliable way to improve the catalytic performance of Fe-based catalysts [46,48,50–54,58,59,61,72,79,83].

(1) Cu Promoter

The addition of Cu to Fe-based catalysts can generally facilitate the reduction and dispersion of Fe active species. For example, Liu et al. [50] investigated the effects of the Cu content on the catalytic performance of Fe-Cu-K/Al_2O_3 catalysts and found that with the increase in the Cu content from 0 to 3%, the light olefin ($C_2^=$–$C_4^=$) selectivity decreased from 20.3 to 14.5%, while the C_{5+} hydrocarbon selectivity significantly increased from 5.4 to 13.8%. This can be attributed to the strong interaction between Cu and Fe, which promoted the reduction and dispersion of Fe active species, as confirmed by HR-TEM, H_2-TPR, and CO_2-TPD analyses [35]. Furthermore, DFT calculations by Hwang et al. [48] revealed the synergistic effects of Cu and K for CO_2 hydrogenation over Fe-based catalysts. That is, the Fe-Cu alloy promotes CO_2 activation by reducing the energy required for oxygen removal, and the addition of K causes an increasing carbon binding energy and a decreasing hydrogen binding energy, which facilitates CO formation and C–C coupling over Cu and Fe surfaces, respectively.

In addition, the types of Cu precursors also have important impacts on the catalytic performance of Fe-based catalysts. Choi et al. [52] successfully prepared Fe-Cu catalysts derived from delafossite-$CuFeO_2$ precursors. Compared with pure Fe_2O_3, CuO-Fe_2O_3 mixture, and spinel $CuFe_2O_4$ catalysts, the Fe-Cu catalysts exhibited the optimum performance with CH_4 and C_{5+} hydrocarbon selectivity of 64.9 and 2.1%, respectively. It is because $CuFeO_2$ with the intermediate oxidation state of Cu^+ has a stronger reduction ability than Cu^{2+}, which is conducive to the rapid reduction and carburization of Fe species to form Fe_5C_2 active species.

(2) Co Promoter

The addition of Co with the capability of chain growth to Fe-based catalysts can promote the conversion of CO intermediates and the subsequent selectivity towards long-chain hydrocarbons [34,36,37,58]. For example, 10Fe0.3K0.53Co catalysts successfully prepared by Jiang et al. [58] exhibited excellent catalytic performance with C_{5+} hydrocarbon selectivity of 47% under CO_2 conversion of 54.6%. Moreover, they also investigated the synergistic effects between Fe and Co active sites on the catalytic performance of Fe-based catalysts, which is related to the proximity between the Fe and Co active sites. The distance between the Fe and Co active sites that changed from the nanoscale to meter scale was simulated by three assembly styles of the 15Fe5K/SiC and 8Co/SiC catalysts: powder-mixing, particle-mixing, and layer-by-layer (15Fe5K/SiC and 8Co/SiC catalysts were loaded upstream and downstream, respectively). It was found that as the distance between the Fe and Co active phases increased, the C_{5+} hydrocarbon selectivity decreased from 30.5% to 2.6%, corresponding to a sharp increase in CH_4 selectivity from 50.6% to 90.2%. That is, the intimate distance between Fe and Co can generate high CO concentrations on the Co active sites, which favors the formation of C_{5+} hydrocarbons via the FTS route. By contrast, the increasing distance between Fe and Co can generate low CO concentrations on the Co active sites, leading to a low C/H ratio, which favors the formation of CH_4.

A suitable proximity between Fe and Co strongly associated with synergistic effects is essential to obtain high CO_2 conversion and C_{5+} hydrocarbon selectivity. However, it is not clear whether the proximity of the Fe-Co mixture is maintained all the time due to the transformation of Fe species during the CO_2 hydrogenation process. Hwang et al. proposed a strategy to stabilize the Fe-Co bimetallic structure [36] in which TMPP cobalt (II) (Co-TMPP) precursors were used as Co-NC supports, and the prepared FeK/Co-NC catalysts had a CO_2 conversion of 51.7% and C_{5+} hydrocarbon selectivity of 42.4%. Compared with the FeK/Co-NC catalysts, the FeCoK/NC catalysts prepared with NC supports exhibited a lower C_{5+} hydrocarbon selectivity of 28.8%. Furthermore, TEM-EDS mapping was characterized for the FeK/Co-NC and FeCoK/NC catalysts to visualize the degree of difference in the formation of the Fe-Co alloy as shown in Figure 2. FeK/Co-NC accounted for 14–27% Co nanoparticles (NPs), whereas FeCoK/NC has a relatively small amount of Co NPs that varies from 3% to 13% (Figure 2a). The difference in alloying degree

was more pronounced. As shown in Figure 2b, after both catalysts underwent the CO_2 hydrogenation reaction for 70 h, and the spent FeK/Co-NC catalyst maintained uniform Fe-Co alloyed structures containing ~20% Co. However, the Fe-Co alloyed structures in the FeCoK/NC catalyst were dealloyed, with Co compositions of 3–60%. This indicates that the Fe-Co alloy in the FeCoK/NC catalysts tended to break away from the alloyed state to Co clusters during the CO_2 hydrogenation process, which reduced the chain growth ability, whereas the Co-NC supports effectively induced the formation of the Fe-Co alloy (Figure 3), which contributed to improving the C_{5+} hydrocarbon selectivity.

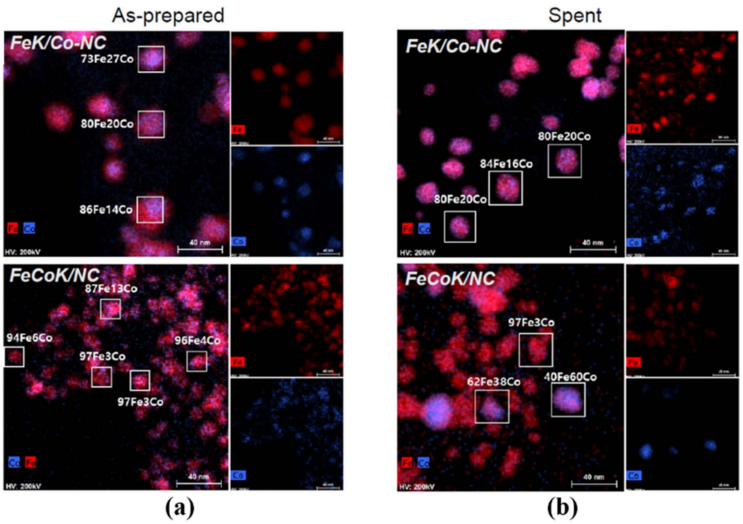

Figure 2. TEM-EDS mapping images of (**a**) as-prepared FeK/Co-NC and FeCoK/NC and (**b**) spent FeK/Co-NC and FeCoK/NC catalysts after reaction for 70 h. Reprinted with permission from Hwang et al. [36]. Copyright (2021) American Chemical Society.

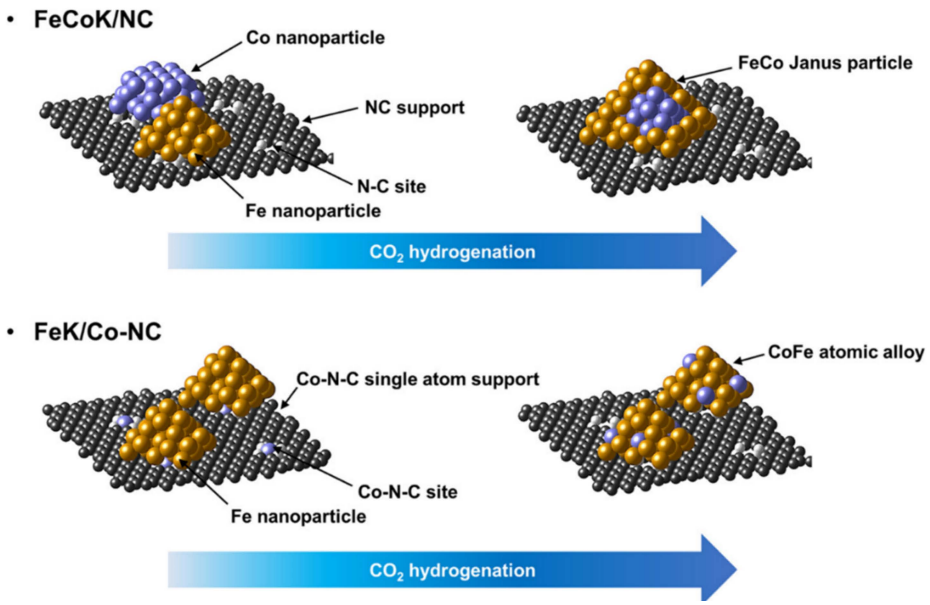

Figure 3. Proposed structures of the FeCoK/NC and FeK/Co-NC catalysts after CO_2 hydrogenation Reprinted with permission from Hwang et al. [36]. Copyright (2021) American Chemical Society.

(3) Zn Promoter

Similar to Cu, Zn [40,59,61,84] acts as a structural promoter [38,39] in the Fe-based catalysts and can generally facilitate CO_2 adsorption as well as subsequent conversion. This can be attributed to the dispersion of Fe active species caused by the interaction between Zn and Fe. However, too strong an interaction inhibits the reduction of Fe species [59,61], which

is not conducive to the production of long-chain hydrocarbons. To deal with this difficulty, strategies of synergistic interactions by combining Zn with Na have been proposed by Zhang et al. [40]. The CO_2 and H_2 adsorption properties of the reduced Fe catalysts (pure Fe, Zn-Fe, Na-Fa, and Na-Zn-Fe catalysts) were investigated using CO_2-TPD (Figure 4a) and H_2-TPD (Figure 4b), respectively. For CO_2 adsorption, the addition of Zn to Na-Fe catalysts significantly strengthened the α and β peaks [60]. As For Na-Fe catalysts, apart from the α and β peaks, a γ peak appeared at around 886 K, which corresponds to the interaction between the CO_2 and alkaline sites increased by Na addition, thus enhancing CO_2 adsorption [60,85]. Furthermore, the introduction of Zn to Na-Fe catalysts particularly increased the strong CO_2 adsorption at the γ peak, which can be explained as follows: Zn reduces the particle sizes of Na-Zn-Fe catalysts. As for the H_2 adsorption, the peaks centered at 645–659 K and 773–826 K were attributed to weak H_2 adsorption [49,86] and the dissociative or subsurface H_2 adsorption [87,88] on the catalyst surface, respectively. It can be seen that the addition of Zn significantly enhanced the amounts of dissociative and weak H_2 adsorption, which promoted the activity of CO_2 hydrogenation.

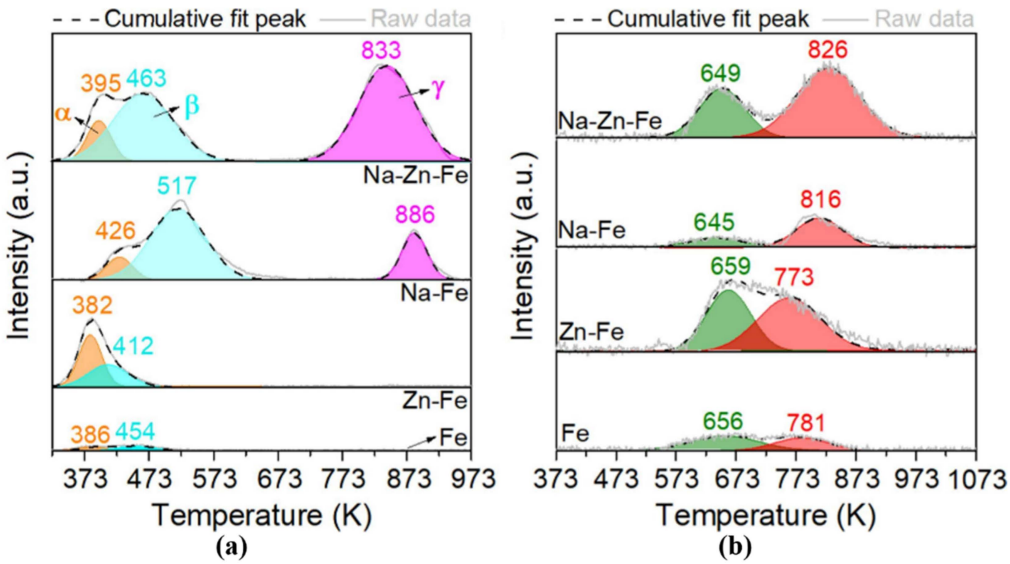

Figure 4. (**a**) CO_2-TPD and (**b**) H_2-TPD profiles of the reduced Fe-based catalysts. Reprinted with permission from Zhang et al. [40]. Copyright (2022) Elsevier.

In other words, the addition of Zn not only significantly reduces the particle size of the Fe active species but also improves the capacity of H_2 adsorption, which is favorable for CO_2 conversion. In addition, co-modification of the Na promoters significantly contributes to the formation of active Fe_5C_2 during the CO_2 hydrogenation process, which is conducive to the formation of long-chain hydrocarbons.

2.1.3. Catalyst Supports

Catalyst supports also play a key role in improving the catalytic activity and catalyst stability [89] because the interaction between the supports and Fe species can inhibit the agglomeration of Fe active sites. Currently, traditional supports such as Al_2O_3 [16], TiO_2 [33,58], SiO_2 [50,57], and ZrO_2 [44] have been investigated for CO_2 hydrogenation via the FTS route, among which Al_2O_3 is mainly used as Fe-based catalyst supports. For example, Song et al. investigated the effects of Al_2O_3 supports on the catalytic performance of FeK/Al_2O_3 catalysts and found that Al_2O_3 with hydroxyl groups facilitates the dispersion of Fe particles and the adsorption of CO intermediates [90], which contributed to the formation of small particles of iron carbide and the improved catalytic performance. Furthermore, amorphous AlO_x phases, as additional active sites, were recently proposed by Khan et al. [49]. Herein, the amorphous AlO_x phases, on the one hand, enhance the adsorption of CO_2 and H_2, thereby improving CO_2 conversion; on the other hand, these

phases provide sites for olefin readsorption, which is beneficial for enhancing long-chain hydrocarbon selectivity.

In addition, there is a suitable range for the pore size of Al_2O_3 supports, considering the catalytic activity and selectivity. Xie et al. reported that a Al_2O_3 pore size of 7–10 nm was the optimal active size for hydrogenation of CO_2 to hydrocarbons [45]. Outside this range, the increase in the pore size of the Al_2O_3 supports led to an increase in the Fe_2O_3 particle size, reducing the dispersion of the Fe active sites. However, the smaller pore size of the Al_2O_3 supports led to too small Fe_2O_3 particle sizes, which cannot favor the carbon chain growth on the catalyst surface. Therefore, it is important to select a support with a suitable pore size.

In recent years, carbon materials with hydrophobicity and excellent carburized ability have been applied as supports, such as mesoporous carbon [68], carbon nanotubes (CNTs) [65–67], and carbon materials based on the pyrolysis of Metal–Organic Frameworks (MOFs). Herein, mesoporous carbon with a mesoporous structure can provide favorable conditions for the rapid diffusion of long-chain hydrocarbons. However, unlike mesoporous carbon, CNTs with tubular structures can provide a high C/H ratio of sites to facilitate carbon chain growth. This is because the outer walls of CNTs naturally possess an electron-rich structure; this structure favors CO_2 adsorption and relatively inhibits H_2 adsorption [65]. Therefore, CNTs have a promising application in the field of CO_2 hydrogenation. Moreover, MOFs have been used as effective precursors for the preparation of carbon supports due to their high surface area and adjustable pore size [91,92]. Guo et al. first pyrolyzed Fe-MIL-88B into Fe-based catalysts [62], which exhibited a CO_2 conversion rate of 46% but high CH_4 selectivity of 26.6%. They also prepared NC materials containing Zn promoters by pyrolyzing ZIF-8 precursors [61], and their supported Fe catalysts show considerable olefin selectivity of 30%. However, in order to obtain high catalytic activity and long-chain hydrocarbon selectivity, regulation or modification of the structure and composition of MOF-based catalysts need to be further explored.

2.1.4. Preparation Methods

Preparation methods are directly relevant to the distribution of catalyst components, which is crucial to regulate the interaction between Fe active sites and other components (i.e., supports and promoters). Herein, representative catalysts prepared by different preparation methods and their catalytic performance are illustrated in Table 3.

Table 3. Representative catalysts prepared by different preparation methods and their catalytic performance for CO_2 hydrogenation.

Entry	Catalysts	Reaction Conditions						Hydrocarbon Distribution (%)						
		H_2/CO_2 Ratios	T (°C)	P (MPa)	GHSV/ $mL \cdot g^{-1} \cdot h^{-1}$	CO_2 Conv. (%)	CO Sel. (%)	CH_4	C_{2-4}	$C_{2-4}{}^{0\,a}$	$C_{2-4}{}^{=\,a}$	C_{5+}	O/P [b]	Ref.
Co-precipitation Methods														
1	Fe-Cu-K-Al	3.0	300	2.5	5000	35.7	N.A.	N.A.	N.A.	N.A.	N.A.	50.7	N.A.	[48]
2	$FeAlO_x$-5	3.0	330	3.5	4000	36.8	7.2	12.1	30.1	N.A	N.A	57.8	N.A	[49]
3	CMO-10	3.0	270	4.0	4000	64.3	0.2	44.2	22.9	N.A.	N.A.	32.9	N.A.	[29]
4	Co-Fe-0.81Na	3.0	240	3.0	5500	10.2	5.2	17.8	9.4	N.A.	N.A.	72.9	N.A.	[28]
Incipient Wetness Impregnation (IWI) Methods														
5	Fe0.17Cu1K/Al_2O_3	3.0	300	1.1	3600	29.3	17.0	8.4	26.5	N.A.	N.A.	65.1	N.A.	[51]
6	10Fe0.8K0.53Co	3.0	300	2.5	560	54.6	2.0	19.3	32.8	7.9	24.9	48.0	3.2	[58]
7	FeK/Co-NC	3.0	300	2.5	N.A.	51.7	21.6	N.A.	N.A.	N.A.	N.A.	42.4	N.A.	[36]
8	FeK/MPC	3.0	300	2.5	2000	50.6	8.2	16.8	34.7	N.A.	N.A.	48.5	N.A.	[68]
Template-assisted Synthesis Methods														
9	Fe_2O_3-CT600	3.0	350	1.5	1140	40.0	15.0	14.1	43.5	N.A.	N.A.	42.4	N.A.	[42]

Table 3. *Cont.*

Entry	Catalysts	Reaction Conditions					Hydrocarbon Distribution (%)							
		H_2/CO_2 Ratios	T (°C)	P (MPa)	GHSV/ $mL \cdot g^{-1} \cdot h^{-1}$	CO_2 Conv. (%)	CO Sel. (%)	CH_4	C_{2-4}	$C_{2-4}{}^{0\,a}$	$C_{2-4}{}^{=\,a}$	C_{5+}	O/P [b]	Ref.
Sol–Gel Methods														
10	Na-Zn-Fe	3.0	340	2.5	15,000	39.0	14.0	12.0	47.7	4.7	43.0	40.5	9.8	[40]
Hydrothermal Synthesis Methods (HSM)														
11	$CuFeO_2$-6 [c]	3.0	300	1.0	1800	17.3	31.7	2.6	31.0	N.A.	N.A.	66.3	7.3	[52]
12	Na-$ZnFe_2O_4$	3.0	340	1.0	1800	34.0	11.7	8.6	28.1	N.A.	N.A.	51.6	11.3	[59]
Organic Combustion Methods (OCM)														
13	Fe-Mn-K	3.0	300	1.0	2400	38.2	5.6	10.4	27.7	N.A.	N.A.	61.7	N.A.	[56]

[a] Meaning paraffins(o) and olefins (=) in C_2–C_4, respectively, [b] Olefins/paraffins ratio of C_2-C_4 products, [c] Containing 0.03% sodium by mass fraction.

Currently, Incipient Wetness Impregnation (IWI) methods are commonly used to prepare efficient catalysts [47,48]. The IWI methods are effective in uniformly dispersing Fe species and promoters on the supports (Figure 5a–d) [50]. Compared with IWI methods, co-precipitation methods can also regulate the particle sizes of Fe species (Figures 5e and 6) and pore sizes of supports by changing the pH values of the reaction solution, stirring speed, and aging time. This provides a feasible pathway to prepare Fe-based catalysts with high activity.

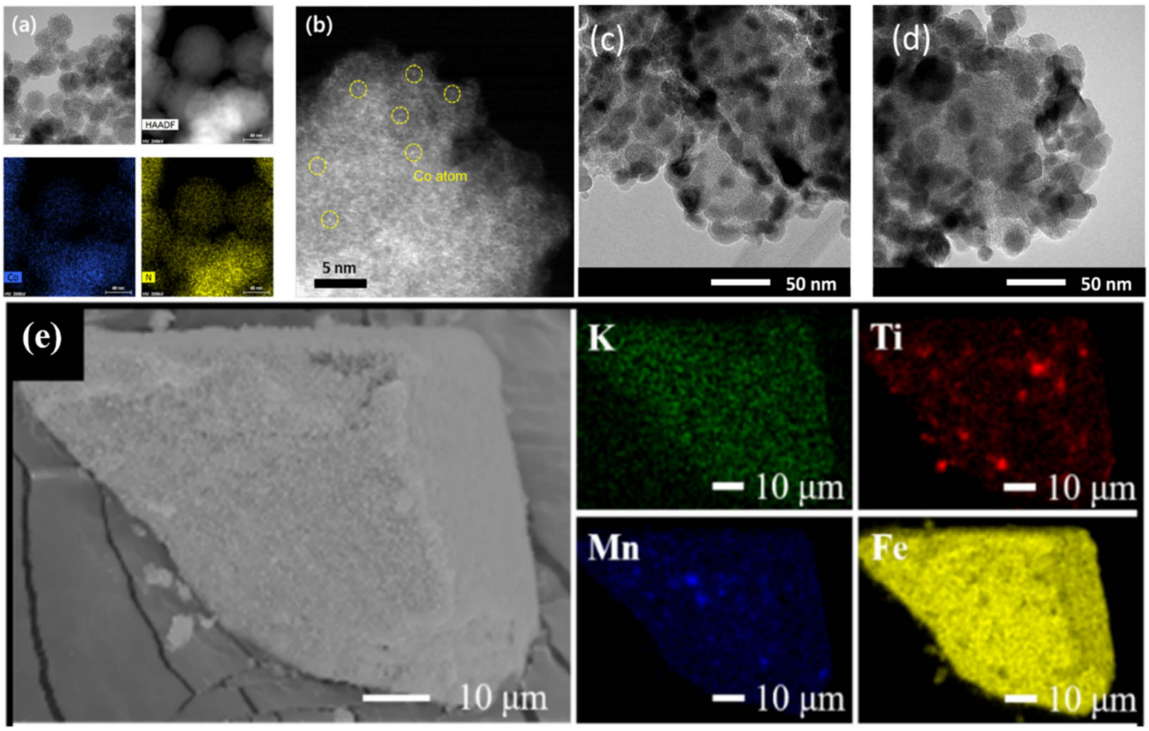

Figure 5. (**a**) TEM-EDS mapping images, (**b**) HADDF-STEM images of atomic Co incorporated in the matrix of Co–NC SAS acquired by Cs-STEM at a higher magnification. Reprinted with permission from Zhang et al. [36]. Copyright (2022) Elsevier. TEM images of (**c**) Fe/MPC and (**d**) FeK/MPC catalysts. Reprinted with permission from Hwang et al. [68]. Copyright (2020) Elsevier. (**e**) FE-SEM images and EDS mappings of $K_3/FeMn_{10}Ti_{20}$. Reprinted with permission from Zhao et al. [57]. Copyright (2021) Elsevier.

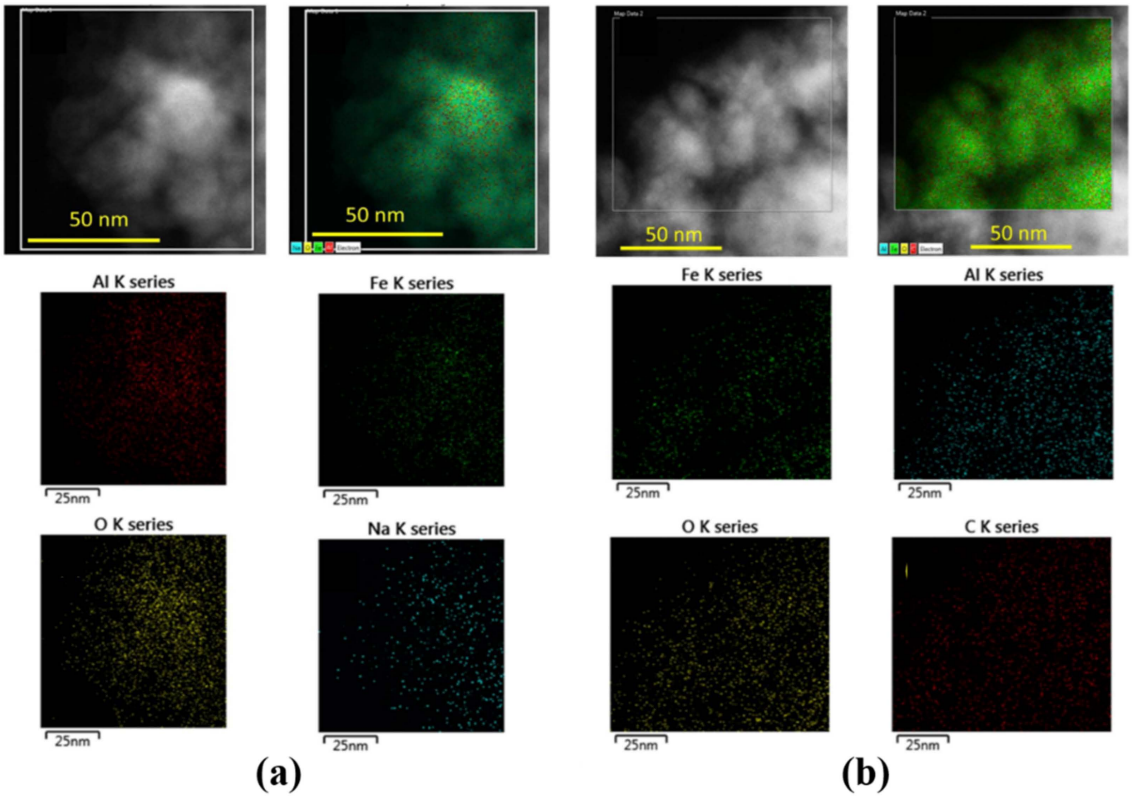

Figure 6. TEM-EDS images of the reduced (**a**) and spent (**b**) $FeAlO_x$-5 catalysts. Reprinted with permission from Khan et al. [49]. Copyright (2020) American Chemical Society.

In addition, other methods such as Hydrothermal Synthesis Methods (HSM) and Organic Combustion Methods (OCM) have been reported to prepare catalysts [16,40,42,52,59,64,93]. HSM are generally conducted under high-temperature and high-pressure conditions. Catalysts prepared by HSM mostly have spinel structures (e.g., $ZnFe_2O_4$ [59] catalysts), which can inhibit the sintering of Fe species during the heat-treatment process and improve the stability of the catalysts during the CO_2 hydrogenation process. Recently, OCM have been applied in the CO_2 hydrogenation field. A citric acid-based slurry containing Fe, Mn, and K precursors was ignited to prepare FeMnK catalysts [56] (Equations (4) and (5)), which exhibited excellent catalytic performance with CO_2 conversion (38.2%) and C_{5+} hydrocarbon selectivity (58.4%). The main advantages of OCM are as follows: (1) The vaporization of water consumes the released heat, limiting the rapid rise of temperature and reducing the local sintering of metal oxide particles. (2) The releases of N_2 and CO_2 are conducive for the high-dispersion preparation of catalysts [94].

$$54\ Fe(NO_3)_3 9H_2O + 46\ C_6H_8O_7H_2O \rightarrow 18\ Fe_3O_4 + 81\ N_2 + 276\ CO_2 + 716\ H_2O \quad (4)$$

$$9\ Mn(NO_3)_2 4H_2O + 5\ C_6H_8O_7H_2O \rightarrow 9\ MnO + 9\ N_2 + 30\ CO_2 + 61\ H_2O \quad (5)$$

2.2. Tandem Catalysts Combined with Fe-Based Active Components and Zeolites

Generally, the aforementioned Fe-based catalysts designed for CO_2 hydrogenation also co-generate $C_2^=$–$C_4^=$, along with the targeted long-chain hydrocarbons. Therefore, tandem catalysts combined with Fe-based active components and zeolites have been adopted to improve the selectivity of long-chain hydrocarbons via further conversion of the $C_2^=$–$C_4^=$ into long-chain hydrocarbons over the acid sites of zeolites through a series of reactions such as oligomerization, isomerization, and aromatization [95–97]. The tandem catalysts can not only improve the selectivity towards long-chain hydrocarbons but also increase the research octane number (RON) of liquid fuels.

For the tandem catalysts, the final distribution of the hydrocarbon products heavily depends on the pore structure and acidity of zeolites. For instance, HMCM-22 with the MWW structure and Hβ with the BEA structure benefit the isomerization and alkylation of olefins [98,99], while HZSM-5 with the MFI structure favors the aromatization of olefins. As for the roles of acidity, Wei et al. revealed that HZSM-5 zeolites with strong BAS were conducive to olefin aromatization [100], while HMCM-22 and Hβ zeolites with medium BAS promoted olefin isomerization. Guo et al. indicated that eliminating the surface-strong Brønsted acids of HZSM-5 by using ion-exchange methods (K^+, Na^+, etc.) is beneficial for improving the selectivity towards C_{5+} long-chain hydrocarbons and suppressing the formation of short-chain saturated hydrocarbons [71]. In addition, a possible reaction pathway for the hydrogenation of CO_2 into iso-paraffins over a Na-Fe_3O_4/HMCM-22 catalyst (Figure 7a) was proposed by Wei et al.

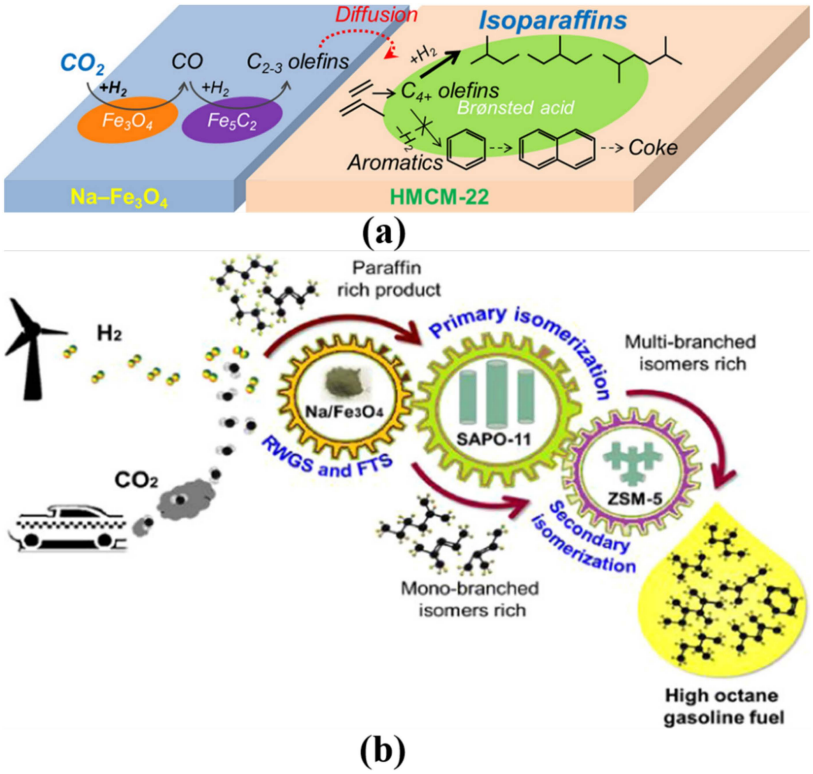

Figure 7. (**a**) Reaction scheme of iso-paraffin synthesis and coke formation during CO_2 hydrogenation over Na-Fe_3O_4/HMCM-22 catalysts. Reprinted with permission from Wei et al. [100]. Copyright (2018) American Chemical Society. (**b**) Reaction scheme of gasoline synthesis formation during CO_2 hydrogenation over NaFe+SAPO-11 + HZSM-5 catalysts. Reprinted with permission from Noreen et al. [70]. Copyright (2020) American Chemical Society.

In addition to the use of tandem catalysts, the use of a multiple-bed reaction system is another effective way to improve the selectivity towards long-chain hydrocarbons. For example, Noreen et al. designed a tri-bed tandem NaFe + SAPO-11 + HZSM-5 catalytic reaction system for gasoline synthesis via CO_2 hydrogenation (Figure 7b) [70], where the mono-branched hydrocarbons were generated over NaFe + SAPO-11, which undergoes secondary isomerization over HZSM-5, therefore improving the selectivity of multibranched hydrocarbons. In this case, the gasoline selectivity reached 71.7% under a CO_2 conversion rate of 31.2%. Moreover, the produced gasoline had an RON value of 91.7, with the selectivity of mono- and di-branched hydrocarbons of 25.7 and 12.5%, respectively (Figure 8a,b).

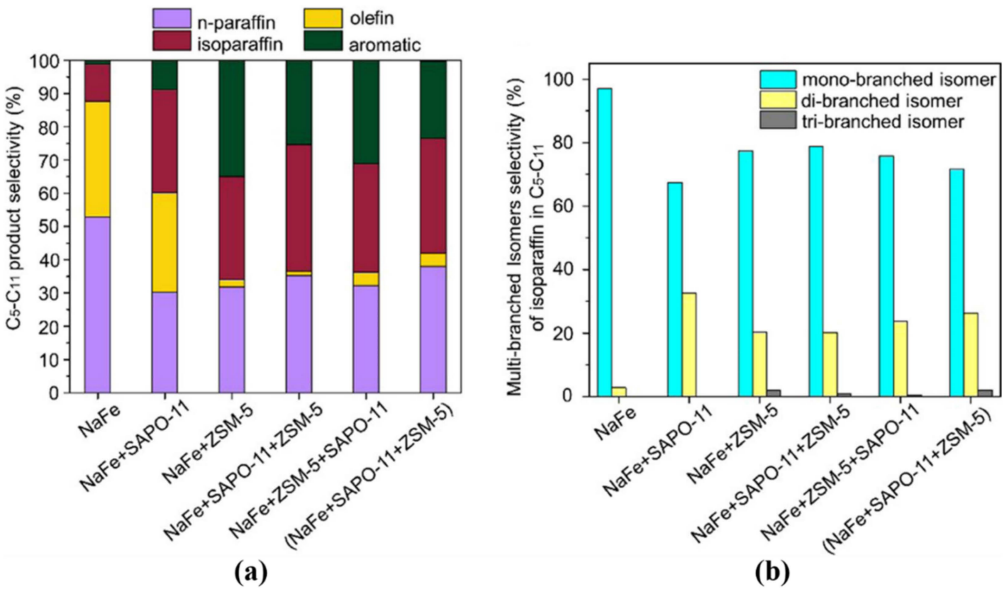

Figure 8. CO_2 hydrogenation over NaFe coupled with HZSM-5 and SAPO-11 for gasoline (C_5–C_{11}) synthesis: (**a**) hydrocarbon distribution and (**b**) branched isomer selectivity in iso-paraffins. Note: "(A + B + C)" means a physical mix of A, B, and C catalysts, "A + B" denotes the sequential addition of A and B catalysts (dual bed), and "A + B + C" symbolizes sequential addition of A, B, and C catalysts (triple bed). Reaction conditions: 320 °C, 3.0 MPa, W_{NaFe}/F = 6 g_{cat}·h/mol, H_2/CO_2 = 3. Reprinted with permission from Noreen et al. [70]. Copyright (2020) American Chemical Society.

2.3. Effects of Reaction Conditions on Catalytic Performance

In general, the reaction conditions (the reaction temperature, reaction pressure, space velocity, and H_2/CO_2 ratio) have significant impacts on the catalytic performance of CO_2 hydrogenation (i.e., CO_2 conversion, selectivity towards targeted hydrocarbons, and catalyst stability). In addition, in the case of the tandem catalysts, the mixing mode of different active components is also an important factor. The relevant content will be discussed below in more detail.

2.3.1. Reaction Temperature

In general, there is an optimum temperature range for CO_2 hydrogenation via the FTS route, that is, too low or too high temperatures are not preferred. This is because the RWGS reaction is endothermic, which favors high temperatures to enhance equilibrium CO_2 conversion, while the FTS reaction is exothermic, which prefers low temperatures to achieve low CH_4 selectivity [101]. Therefore, increasing reaction temperatures can improve CO_2 conversion, but this may result in a decrease in the selectivity towards C_{5+} long-chain hydrocarbons [102,103]. As seen in Figure 9a, as the temperatures increased from 300 to 360 °C, the CO_2 conversion increased by about 20%. However, when the temperature further increased to 380 °C, the CO_2 conversion only slightly increased by 1.2%, but C_{5+} long-chain hydrocarbon selectivity significantly decreased by 9.8%. Therefore, it is important to seek an optimum temperature range to obtain optimized catalytic performance for CO_2 hydrogenation by balancing the RWGS and FTS reactions.

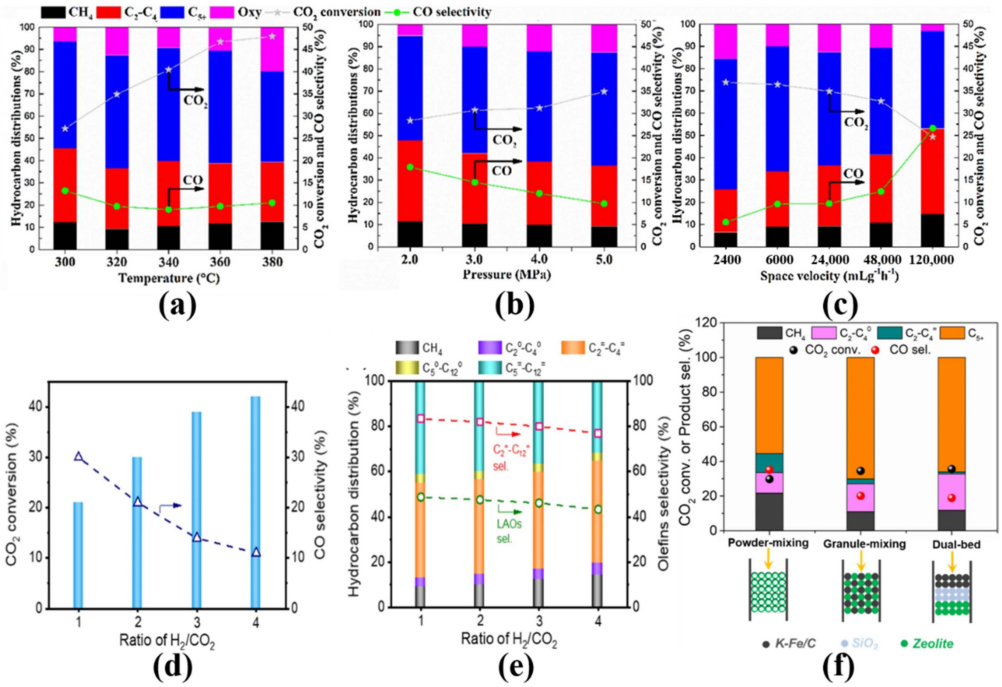

Figure 9. The catalytic performance of the $K_3/FeMn_{10}Ti_{20}$ catalysts under various conditions: temperature (**a**), pressure (**b**), and space velocity (**c**) in CO_2 hydrogenation ($H_2/CO_2/Ar$ = 70.00 v%/25.03 v%/4.97 v%). Reprinted with permission from Zhao et al. [57]. Copyright (2021) Elsevier. Effects of H_2/CO_2 on catalytic performance (**d**) and hydrocarbon distribution (**e**). Reaction conditions: 340 °C, 2.5 MPa, GHSV = 15,000 mL·g_{cat}^{-1}·h^{-1}, TOS = 10 h. Reprinted with permission from Zhang et al. [40]. Copyright (2022) Elsevier. (**f**) Effects of the mixing mode on the catalytic performance of a tandem catalyst coupled with K-Fe/C and zeolite. Reaction conditions: 320 °C, 2.0 MPa, GHSV = 1200 mL·g_{cat}^{-1}·h^{-1}, H_2/CO_2 = 2.5, mass ratio of K-Fe/C to zeolite = 1/3. Reprinted with permission from Guo et al. [71]. Copyright (2021) Elsevier.

2.3.2. Reaction Pressure

Generally, high reaction pressures are beneficial for improving both the CO_2 conversion and the selectivity towards long-chain hydrocarbons. This is because the CO_2 hydrogenation reaction decreases in moles, so high pressure facilitates CO_2 conversion from the thermodynamic point of view. As shown in Figure 9b, as the reaction pressure increased from 2 to 5 MPa, the CO_2 conversion over the $K_3/FeMn_{10}Ti_{20}$ catalysts increased from 28.4% to 34.9%. Meanwhile, its chain growth capacity was also enhanced, leading to a decrease in CO selectivity and an increase in the selectivity towards C_{5+} long-chain hydrocarbons. This is mainly because of the enlarged amount of surface C* species under high pressure, which benefits the generation of iron carbide active sites for long-chain hydrocarbon synthesis [104].

2.3.3. Space Velocity

In addition to the reaction temperature and pressure, space velocity is also an important factor because it affects the residence time of the reactants and thus the catalytic performance of the catalysts. As shown in Figure 9c, the CO_2 conversion sharply decreased with increasing space velocity, which is because of the insufficient adsorption and activation of CO_2 within a short contact time. Moreover, with the increase in space velocity from 2400 to 120,000 mL·g_{cat}^{-1}·h^{-1}, the product distribution shifted to short-chain hydrocarbons. This is mainly because the short contact time between reactants and Fe active sites inhibits the secondary hydrogenation reaction.

2.3.4. H_2/CO_2 Ratio

CO_2 is chemically very stable; therefore, increasing the active component H_2 can promote CO_2 activation and subsequent conversion. As seen in Figure 9d, the CO_2 conversion increased markedly from 21% to 42% over the Na-Zn-Fe catalysts, along with a significant decrease in the CO selectivity from 30% to 11% as the H_2/CO_2 ratio increased from 1 to 4, but a H_2/CO_2 ratio that is too high has an obvious effect on the hydrocarbon distribution. Increasing the H_2/CO_2 ratio resulted in a decrease in $C_5^=$–$C_{12}^=$ selectivity from 41% to 32% (Figure 9e), which was mainly caused by the subsequent hydrogenation of olefins under a high H_2 atmosphere [105,106] considering the situation that the value of O/P decreased from 11 to 8.4 [40]. Therefore, an appropriate H_2/CO_2 ratio should be determined with reference to CO_2 conversion and long-chain hydrocarbon selectivity.

2.3.5. Mixing Mode of Different Active Components

The mixing mode of different active components has significant effects on the catalytic performance for CO_2 hydrogenation. As shown in Figure 9f, the K-Fe/C and K-ZSM-5 catalysts in the granule-mixing mode exhibited an excellent liquid fuel selectivity of 70.1%, where the olefin intermediates formed over the K-Fe/C active sites underwent a series of reactions such as oligomerization, isomerization, and aromatization over the acid sites of K-ZSM-5 due to an appropriate distance between the different active sites. However, compared with the granule-mixing mode, the K-Fe/C and K-ZSM-5 catalysts in the powder-mixing mode exhibited lower CO_2 conversion and C_{5+} hydrocarbon selectivity. This is because K promoters on the K-Fe/C catalyst poison the acidic sites of zeolites due the close proximity, which lessens the synergistic effects [69].

3. Hydrogenation of CO_2 to Aromatics over FeO_x/Zeolite Tandem Catalysts

Aromatics, as important raw materials, can be used to prepare polymers, medicines, paints, and so on. With the rapid social and economic development, the demands for aromatics are increasing. Generally, the traditional aromatic production process is heavily dependent on fossil energy, which results in considerable CO_2 emissions [107–109]. Therefore, hydrogenation of CO_2 to aromatics is regarded as a promising way for the sustainable synthesis of aromatics [108].

The reaction pathway for hydrogenation of CO_2 to aromatics via the FTS route is illustrated in Figure 10, coupled with Fe-based catalysts and zeolites, named as FeO_x/zeolite tandem catalysts hereafter. Then, olefin intermediates form over the Fe active sites by RWGS and FTS (Equations (2) and (6)), and can be further converted into aromatics by aromatization over the acid sites of zeolites (Equation (7)) [60,104]. As also mentioned above, the Fe-based catalysts generally have both RWGS and FTS activity [110], and after appropriate modification (addition of promoters, introduction of supports, and improvement of preparation methods), they have low CH4 and high olefin selectivity under high temperatures. Therefore, this part focuses on the discussion of zeolite. Herein, the recent progress of the tandem catalysts for the hydrogenation of CO_2 to aromatics is described below in detail, and some representative catalysts as well as their catalytic performances are listed in Table 4.

$$n\,CO + 2n\,H_2 \rightarrow -(CH_2)_n- + n\,H_2O \quad (6)$$

$$C_nH_{2n} \rightarrow {}^{n}/_{m}\,C_mH_{2m-6} + {}^{3n}/_{m}\,H_2 \quad (7)$$

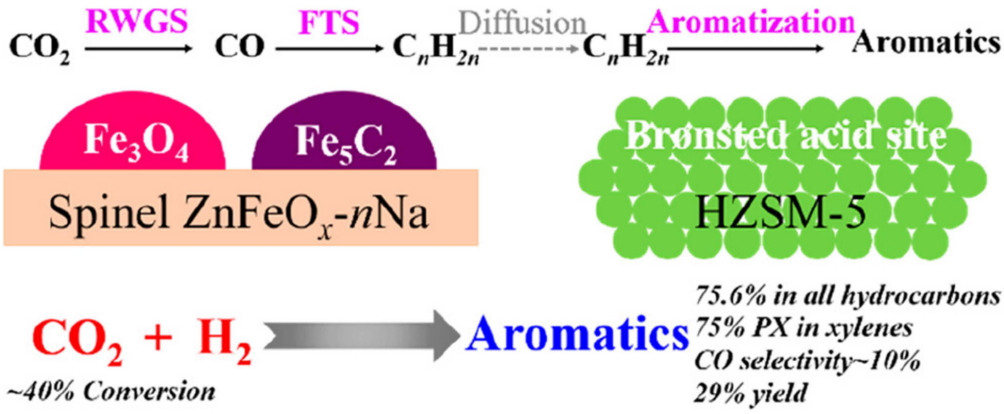

Figure 10. Illustration of the reaction routes of CO_2 hydrogenation to aromatics over the $ZnFeO_x$-nNa/HZSM-5 catalysts. Reprinted with permission from Cui et al. [60]. Copyright (2019) American Chemical Society.

Table 4. Representative catalysts and their performance for direct hydrogenation of CO_2 to aromatics.

Entry	Catalysts	Reaction Conditions				CO_2 Conv. (%)	CO Select. (%)	Hydrocarbon Distribution (%)					
		H_2/CO_2 ratios	T (°C)	P (MPa)	GHSV /mL·g^{-1}·h^{-1}			CH_4	C_{2-4} [a]	Aro. [b]	C_{5+} [c]	Yield	Ref.
1	Na/Fe-HZSM-5	3.0	300	1.0	4800	21.8	40.9	14.7	25.5	54.7	5.1	22.4	[104]
2	1Na-Fe/HZSM-5	3.0	340	3.0	4000	32.3	16.6	5.6	19.9	63.5	11.2	20.4	[111]
3	K-3Fe/Zn/ HZSM-5(21)	3.0	320	3.0	7200	43.6	11.5	13.6	23.3	25.4	37.7	11.1	[96]
4	15Fe-10K/ Al_2O_3&P-HZSM-5	1.0	400	3.0	6000	36.4	10.2	10.8	39.6	39.5	10.1	14.4	[95]
5	FeK1.5/ HSG | HZSM-5(50)	3.0	340	2.0	26,000	35.0	39.0	3.5	4.4	68.0	24.0	23.8	[112]
6	$ZnFeO_x$-4.25Na/ HZSM-5	3.0	320	3.0	4000	36.2	6.9	11.1	16.5	60.0	15.6	21.8	[60]
7	Na-Fe@C/ H-ZSM-5	3.0	320	3.0	6000	33.3	13.3	4.8	10.4	50.2	34.6	16.8	[113]
8	Na-Fe_3O_4/ HZSM-5	2.0	320	3.0	4000	27.7	16.0	5.9	29.6	44.5	20.0	12.3	[114]
9	6.25Cu-Fe_2O_3/ HZSM-5-pt	3.0	320	3.0	1000	55.4	4.41	12.5	9.4	61.9	15.4	34.3	[115]
10	6.25Cu-Fe_2O_3/ HZSM-5-dg	3.0	320	3.0	1000	49.7	6.1	20.8	10.5	44.9	22.4	22.3	[115]
11	6.25Cu-Fe_2O_3/ HZSM-5-hy	3.0	320	3.0	1000	54.5	4.45	12.3	10.0	55.2	21.5	30.1	[115]
12	Na–$FeAlO_x$/ Zn-HZSM-5(12.5)@SiO_2	3.0	370	3.0	4000	45.2	15.3	13.8	26.2	38.7	21.3	17.5	[116]
13	2.83Na-FeMn/ HZSM-5(105)	3.0	320	3.0	4000	27.0	21.9	9.0	28.4	36.5	26.1	9.9	[117]
14	Fe_2O_3@KO_2/ ZSM-5	3.0.	375	3.0	5000	47.4	13.7	14.9	45.9	23.9	15.3	11.3	[118]

[a] C_2–C_4 denote hydrocarbons with a carbon number of 2 to 4. [b] Aro. denotes aromatics. [c] C_{5+} denotes C_{5+} hydrocarbons not including aromatics.

3.1. Strategies for Optimizing Product Distribution of Fe-Based Active Components

As mentioned above, for hydrogenation of CO_2 to aromatics via the FTS route, CO_2 was converted to olefin intermediates by RWGS and FTS over the Fe-based active component, and olefins diffuse to the pores of zeolites for the formation of aromatics [119]. Therefore, high olefin intermediate selectivity is a crucial factor to promote the formation of aromatics. However, pure Fe-based catalysts generally have some disadvantages in CO_2 hydrogenation, such as a low yield of olefins and rapid deactivation of Fe active species [120]. To address these issues, several strategies such as the addition of metal

promoters, the selection of suitable catalyst supports, and the optimization of catalyst preparation methods have been widely investigated to further enhance CO_2 conversion and to improve olefin selectivity, which will be summarized below in detail [121].

3.1.1. Metal Promoters

The addition of alkali metals (Na, K, etc.) can promote CO_2 adsorption and its subsequent conversion [46,122]. In addition, the alkali metals also facilitate the reduction of iron oxides and subsequent formation of iron carbides (FTS active sites) [123]. As shown in Figure 11a, Ma et al. prepared a Na-Fe_3O_4 catalyst [111] and found that with the increase in the Na content from 0% to 3%, the CO_2 conversion increased from 15.2% to 26.7% and the $C_2^=$–$C_4^=$ selectivity increased from 6% to 23%. This is mainly because Na, as an electronic promoter, can transfer electrons to the surface of Fe species, which favors CO_2 adsorption and inhibits H_2 adsorption, therefore generating a high surface C/H ratio and facilitating olefin formation. Then, coupling of the 1Na/Fe catalysts with HZSM-5(30) can obtain an aromatic selectivity of 63.5% (Table 4, Entry 2). In addition, the addition of transition metals such as Zn [124] and Cu [51] has been widely used for the modification of Fe-based catalysts, which facilitates the reduction and dispersion of Fe active species. For example, Liang et al. investigated the influence of the Zn content on the catalytic performance of the K-nFe/Zn catalysts (n = 0, 1, 3, and 6 refer to the surface molar ratios of Fe to Zn) [96]. The results indicated that the appropriate loading of Zn (n = 1, 3) can promote the formation of Fe active sites. However, excessive Zn (n > 3) tends to form large ZnO clusters and/or relatively stable $ZnFe_2O_4$ spinels, which are not conducive to the reduction of Fe active species. Moreover, Cu generally has good RWGS activity; therefore, the addition of Cu to Fe-based catalysts may over-promote CO formation. However, as shown in Figure 11b, Song et al. found that as the Cu concentration increased from 0% to 6.25%, CO selectivity decreased from 14% to 3.51%, and the aromatic selectivity increased from 32% to 57.02%. This was mainly attributed to the synergic effects between Cu and Fe species [115]. However, as the Cu concentration further increased from 6.25% to 50%, the CO selectivity increased by 11.49% and aromatic selectivity decreased by 26.02%. Therefore, the addition of adequate metal promoters to Fe-based catalysts is crucial for improving CO_2 conversion and aromatic selectivity.

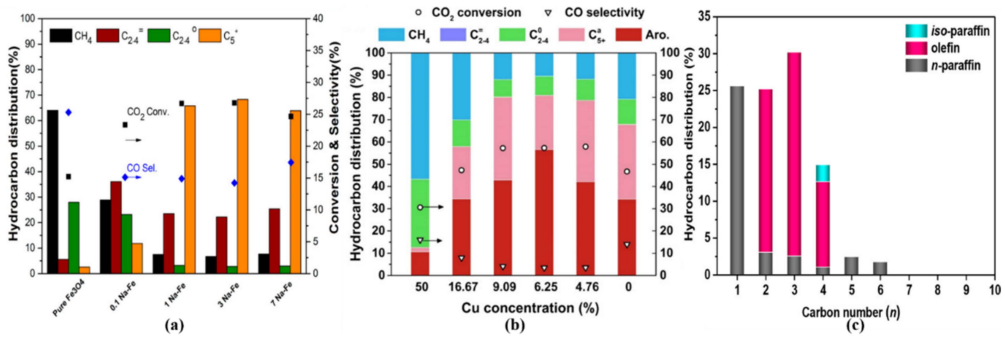

Figure 11. (**a**) Catalytic performance of Na-Fe_3O_4 catalysts with different Na contents. Reaction conditions: 320 °C, 3.0 MPa, GHSV = 4000 mL·g_{cat}^{-1}·h^{-1}, TOS = 48 h. Reprinted with permission from Wen et al. [111]. Copyright (2020) American Chemical Society. (**b**) Hydrocarbon distribution, CO_2 conversion, and CO selectivity over nCu-Fe_2O_3/HZSM-5-c catalysts with various Cu concentrations. HZSM-5-c represents commercial HZSM-5. Reaction conditions: 320 °C, 3.0 MPa, GHSV = 1000 mL·g_{cat}^{-1}·h^{-1}, $H_2/CO_2/N_2$ = 72/24/4, 2 g tandem catalysts. Reprinted with permission from Song et al. [115]. Copyright (2020) American Chemical Society. (**c**) Product distribution over the sole FeK1.5/HSG catalysts. Reaction conditions: 340 °C, 2.0 MPa, GHSV = 26,000 mL·g_{cat}^{-1}·h^{-1} (relative to the total catalyst weight), H_2/CO_2 = 3, 150 mg of FeK1.5/HSG, 150 mg of HZSM-5(50), TOS = 24 h. Reprinted with permission from Wang et al. [112]. Copyright (2019) American Chemical Society.

3.1.2. Catalyst Supports

The surface properties and pore structure of supports (e.g., oxides and carbon materials) have significant impacts on the catalytic performance of Fe-based catalysts. For the surface property, Dai et al. prepared a 15Fe-10K/alkaline-Al_2O_3 catalyst and found that alkaline-Al_2O_3 supports increased the dispersion of the Fe-K bimetals, which inhibited the agglomeration of Fe and K metal particles during calcination. In addition, alkaline-Al_2O_3 also promoted CO_2 adsorption and subsequent conversion, which hindered H_2 adsorption. Therefore, the catalyst surface had a low H_2/CO_2 ratio and promoted light olefin formation [95]. The pore structure of the supports is also a crucial factor for the dispersion of Fe active species. Wang et al. prepared honeycomb-structured graphene (HSG)-supported FeK1.5 catalysts (FeK1.5/HSG) [112,125]. As shown in Figure 11c, the $C_2^=$–$C_4^=$ selectivity reached 59% over the FeK1.5/HSG catalysts. Apart from the promotional effect of the K promoter, the interaction between the HSG supports and Fe active species also promoted olefin formation. Moreover, the FeK1.5/HSG catalysts coupled with the HZSM-5(50) zeolites had an aromatic selectivity of 68%. This can be explained as follows: the large pore size of HSG promotes the free diffusion of reactants and products, which inhibits the secondary hydrogenation of $C_2^=$–$C_4^=$, and therefore a number of light olefins can diffuse to HZSM-5 and be converted to aromatics by aromatization [126].

3.1.3. Preparation Methods

Preparation methods also affect the surface morphology and the property, dispersion, and structure of the Fe active species, resulting in different catalytic performances of Fe-based catalysts. For example, Cui et al. synthesized $ZnFeO_x$-nNa nanocatalysts by a one-pot method [60]. In the process of catalyst preparation, NaOH was used as both a precipitating agent and a promoter source to achieve the preparation and modification of catalysts [24]. The samples with various Na concentrations were obtained by controlling the amount of water in the filtration step. The $C_2^=$–$C_4^=$ selectivity reached 34.8% over the $ZnFeO_x$-nNa catalyst, which was beneficial to obtain an aromatic selectivity of 60% (Table 4, Entry 6). Wang et al. synthesized Fe-MOFs (MIL-88B-Fe) by HSM [113], then prepared Fe-based catalysts (Fe@C) through the pyrolysis of MIL-88B-Fe, and finally obtained Na-Fe@C catalysts by IWI methods. The transmission electron microscopy (TEM) image indicated that the Na-Fe@C catalyst, encapsulated by a few carbon layers, had a core-shell structure, which benefited good dispersion of Fe active species and suppressed their deactivation. Therefore, reasonable improvement of the preparation methods can enhance the catalytic activity of the catalysts.

3.2. Rational Modification of Zeolites

Zeolite is an important part of the tandem catalysts for the hydrogenation of CO_2 to aromatics, which plays a key role in the oligomerization, isomerization, and aromatization of light hydrocarbons. A large number of studies showed that the pore structure, surface acidity, and preparation methods of zeolites have significant effects on the catalytic performance of tandem catalysts [127], which will be summarized below in detail.

3.2.1. Main Influencing Factors of Zeolites

(1) Type of Zeolite

Aromatic selectivity is heavily dependent on the type of zeolite. Wang et al. compared the catalytic performance of different tandem catalysts composed of FeK1.5/HSG catalysts and different types of zeolites (SAPO-34, HY, Hβ, HMCM-22, Na-ZSM-5, HZSM-5, etc.). The results showed that the lowest (3%) and highest (68%) aromatic selectivity values were obtained over SAPO-34 and HZSM-5(50), respectively [112], as seen in Figure 12a. This can be explained by the fact that the pore size of SAPO-34 (3.8 Å × 3.8 Å) is too small; therefore, ethylene (kinetic diameter: 3.9 Å) cannot enter the internal pores of SAPO-34 smoothly, whereas the pore sizes of HZSM-5 (5.1 Å × 5.5 Å and 5.3 Å × 5.6 Å) are similar to the kinetic diameter of aromatics (5–6 Å), which facilitates the diffusion of aromatic products.

Moreover, with an equal SiO_2/Al_2O_3 ratio, compared with HZSM-5(50), NaZSM-5(50) with the exchange degree of 80% has less aromatic selectivity, which indicates that HZSM-5(50) has sufficient acidity to synthesize aromatics. Therefore, HZSM-5 is generally regarded as a preferred zeolite for the hydrogenation of CO_2 to aromatics. In addition, Wei et al. prepared a Na-Fe_3O_4/HZSM-5 catalyst [69], which indicated good catalyst stability maintained within a time on stream (TOS) of 1000 h, as shown in Figure 12b.

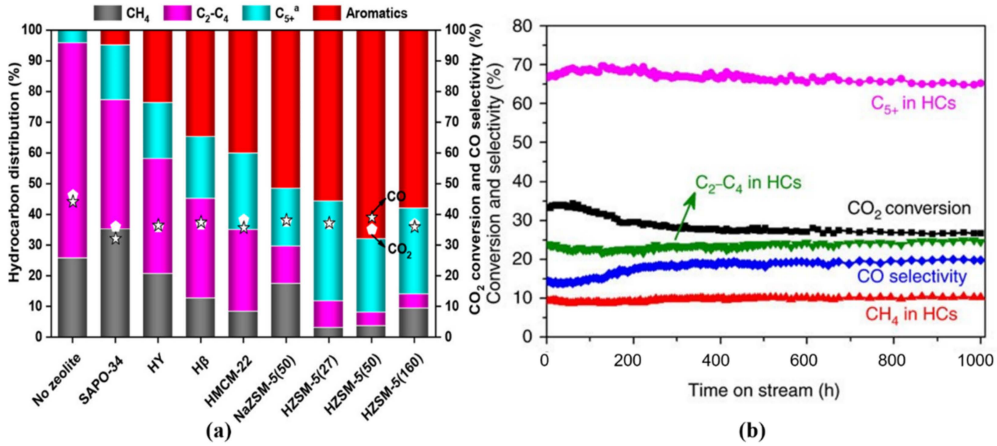

Figure 12. (**a**) Effects of zeolite type on CO_2 conversion and product selectivity over the FeK1.5@HSG/zeolite catalysts. Reaction conditions: 340 °C, 2.0 MPa, GHSV = 26,000 mL·g_{cat}^{-1}·h^{-1}, H_2/CO_2 = 3. Reprinted with permission from Wang et al. [112]. Copyright (2019) American Chemical Society. (**b**) The stability of the Na-Fe_3O_4/HZSM-5 catalysts with dual-bed configuration. Reaction conditions: 320 °C, 3 MPa, GHSV = 4000 mL·g_{cat}^{-1}·h^{-1}, H_2/CO_2 = 3. Reprinted with permission from Wei et al. [69]. Copyright (2017) Springer Nature.

(2) BAS of Zeolites

For the formation of aromatics, the BAS density of zeolites is a key factor, which is closely related to the Si/Al ratio of zeolites [128]. Wei et al. studied the effects of the BAS density of HZSM-5 on the catalytic performance of CO_2 hydrogenation to aromatics [114] and found that with the increase in BAS density from 0 to 356 μmol·g^{-1}, the aromatic selectivity in total hydrocarbons greatly increased from 1.1% to 44.5%. However, it increased at a decreasing rate, and the aromatic selectivity remained stable when the BAS density exceeded 50 μmol·g^{-1}, indicating that the promotional effect of BAS density on aromatization is limited. As for hydrocarbon formation excluding aromatics, with the increase in BAS density from 0 to 356 μmol·g^{-1}, C_2^0–C_4^0 paraffin selectivity monotonously increased by 22.7%, while C_{5+} hydrocarbon selectivity decreased by 9.7%. This is attributed to the cracking of heavy hydrocarbons due to high BAS density. Therefore, a moderate BAS density (i.e., suitable Si/Al ratios) is important for improving the aromatic selectivity and product distribution [118].

(3) Preparation Methods

Preparation methods generally have significant impacts on the pore structure and surface acidity of zeolites, therefore affecting the catalytic performance of tandem catalysts. For example, Cui et al. prepared an HZSM-5 zeolite by a seed-assisted method without using organic templates [60]. Compared with commercial HZSM-5, the as-prepared HZSM-5 had large amounts of mesopores with a suitable BAS density, which facilitated the rapid diffusion of olefin intermediates and/or aromatics, therefore suppressing the formation of coke and improving the catalyst stability. In addition, Song et al. [115] prepared HZSM-5 by various methods such as phase transfer (pt) [129], dry-gel conversion (dg) [130], and hydrothermal synthesis (hy) [131] and found that the highest BTX aromatic selectivity of 54.18% was obtained over 6.25Cu-Fe_2O_3/HZSM-5-pt catalysts, as seen in Figure 13. This is because HZSM-5-pt has abundant mesopores of 5–12 nm, which are favorable for the

formation of BTX. Therefore, the formation of aromatics can be effectively regulated by adjusting the pore structure and surface acidity through proper preparation methods.

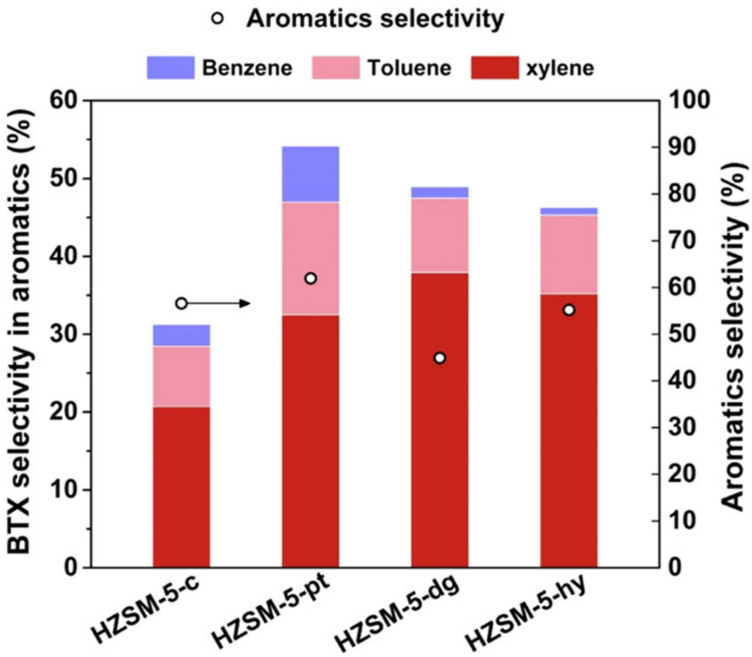

Figure 13. BTX selectivity in aromatics and aromatic selectivity on 6.25Cu-Fe_2O_3 integrated with different HZSM-5 zeolites. Reaction conditions: 320 °C, 3.0 MPa, GHSV = 1000 mL·$g_{cat}{}^{-1}$·h^{-1}, $H_2/CO_2/N_2$ = 72/24/4, 2 g tandem catalysts. Reprinted with permission from Song et al. [115]. Copyright (2020) American Chemical Society.

Therefore, as mentioned above, the types, preparation methods, and BAS density affect the acidity of zeolites. For hydrogenation of CO_2 to aromatics via the FTS route, olefin aromatization is the typical acid-catalyzed reaction. The proper acidity and density can provide active sites for cracking, oligomerization, aromatization, and isomerization of olefin intermediates. However, excessive intensity and density of acid sites can lead to low paraffin formation and/or carbon deposition, which is not conductive to generating aromatics and preparing highly stable catalysts [132].

3.2.2. Strategies for Regulating the Pore Structure and Surface Acidity

The modification of HZSM-5 is mainly to mediate surface acidity, regulate the pore structure, and improve carbon accumulation resistance. In recent years, post-treatment methods such as alkali treatments [132], cationic modification [127], and SiO_2 coating [104] have been widely used to obtain mesopores and suitable BAS density and to passivate the external BAS of HZSM-5.

(1) Alkali Treatments

In general, the as-purchased commercial HZSM-5 only contains micropores, which hinders the rapid mass transfer inside the internal pores of HZSM-5 and causes its easy deactivation [133]. However, HZSM-5 under alkali treatment is beneficial for generating a large number of mesopores and tuning its acidity by redistributing the framework of Al [134]. In general, NaOH solution is used for alkali treatment of HZSM-5. For example, Wang et al. investigated the effects of alkali treatment on the catalytic performance of Na-Fe@C/HZSM-5 tandem catalysts and found that as the concentration of the NaOH solution increased from 0 M to 0.2 M, the aromatic selectivity increased from 30.9% to 50.2%. This is due to the synergistic effects between the appropriate amount of BAS and the hierarchical structure, promoting the formation of aromatics. In addition, the hierarchical structure is conducive to increasing the mass-transfer efficiency, thus inhibiting carbon deposition and

extending the lifetime of the catalysts [113]. In addition, Zhang et al. studied the acidity of alkali-treated HZSM-5 [135] and found that the weak, strong, and total acidity increased after alkali treatment, as shown in Figure 14a. This is due to the fact that the alkali treatment selectively removes the framework of Si, but the Al remains. Compared with commercial HZSM-5, the Lewis acid site (LAS) density of alkali-treated HZSM-5 increased at the cost of BAS density reduction, as shown in Figure 14b. Furthermore, the ZSM-5(50) after alkali treatment had a higher BTEX yield and better stability than commercial HZSM-5(50). In more detail, when the TOS ranged from 0 h to 48 h, the BTEX yield over ZSM-5(50) in the alkali treatment decreased by 5.1%, whereas that over commercial HZSM-5(50) decreased by 15.7%. This can be mainly attributed to the improved total acidity, the increased L/B ratio, and the large amounts of mesopores generated after alkali treatment.

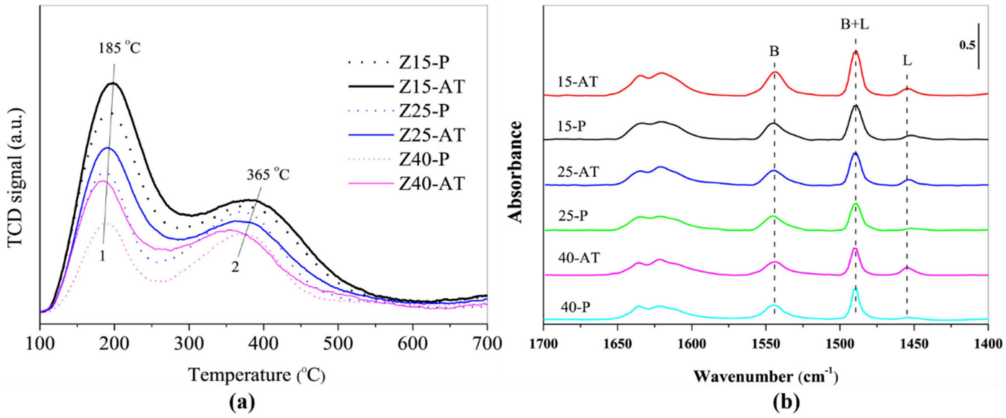

Figure 14. (**a**) NH_3-TPD profiles of the parent and alkali-treated HZSM-5. (**b**) Pyridine FTIR spectra of the parent and alkali-treated HZSM-5. Z15, 25, and 40 denote HZSM-5 with SiO_2/Al_2O_3 ratios of 15, 25, and 40. P denotes parent. AT denotes alkali treatments. Reprinted with permission from Zhang et al. [135]. Copyright (2019) Elsevier.

(2) Modification of HZSM-5

Modification of HZSM-5 via cation substitution (Ga, P, Zn, etc.) is a common approach for tuning its surface acidity, which can be realized by using impregnation or ion exchange methods. More specifically, Dai et al. prepared P-modified HZSM-5 by IWI methods and studied the catalytic performance of Fe-K/alkaline-Al_2O_3 and P/ZSM-5 with different P loadings [95]. They found that as the P loadings increased from 0 wt% to 0.8 wt%, the peak of B acid decreased (Figure 15a), and the aromatic selectivity increased by 2.5%. This can be explained as follows: the P modification increases the amount of medium-strength acid sites, and a moderate P loading is important for the improvement of the acidity and density of zeolites, which can promote the formation of aromatics [136], which promoted the aromatization of ethylene to BTEX aromatics [137]. Moreover, a Zn loading of 0.5 wt% significantly improved the yield of BTEX aromatics (Figure 15b,c), whereas when the Zn loading further increased to 2 wt%, it had negative effects on catalyst stability. Meanwhile, compared with Zn and P, Ga-modified HZSM-5 has a stronger dehydrogenation capacity, which favors paraffin dehydrogenation and subsequent aromatization [138–140].

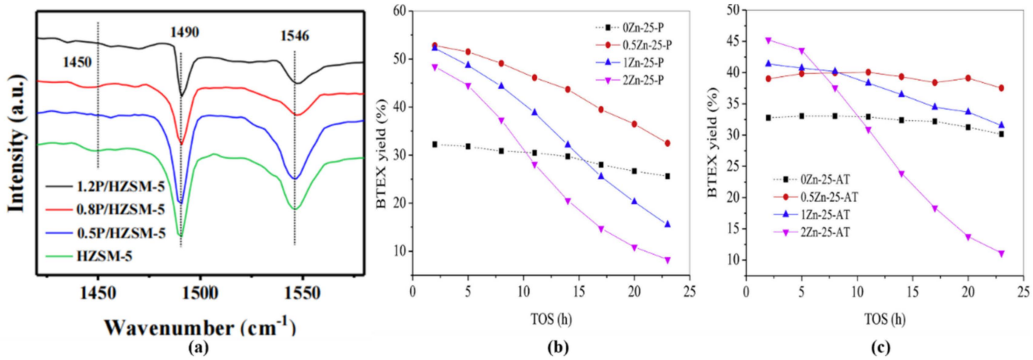

Figure 15. (**a**) FT-IR spectra of HZSM-5 with different phosphorus loadings with pyridine (Py) adsorption at 300 °C. Reprinted with permission from Dai et al. [95]. Copyright (2020) American Chemical Society. (**b**) BTEX yield with TOS of Zn-doped ZSM-5(25)-P and (**c**) Zn-doped ZSM-5(25)-AT. The Zn doping level represents the mass ratio of Zn/Fe, including 0.5%, 1%, and 2%; P—parents; AT—Alkali treatment. Reprinted with permission from Zhang et al. [136]. Copyright (2019) Elsevier.

(3) SiO_2 Coating

Among various aromatics, BTEX aromatics have a higher added value and are widely used as basic raw materials in the current petrochemical industry. Many studies have shown that BTEX aromatics formed on the internal surface acid sites can be further converted to their isomers or even heavy aromatics on the external surface acid sites of HZSM-5 [138]. For example, p-xylene (PX) can be converted to o-xylene (OX) and m-xylene (MX) by isomerization [141,142]. Therefore, in order to enhance the BTEX selectivity, it is necessary to passivate the external BAS of HZSM-5, thus inhibiting the side reactions such as isomerization and over-aromatization [143], which can be realized by coating SiO_2 on the external surface of HZSM-5. For example, Sibi et al. prepared a Na-FeAlO$_x$/Zn-HZSM-5(12.5)@SiO_2 tandem catalyst, in which SiO_2 coating over the external surface of HZSM-5 was conducted by using the chemical liquid phase deposition (CLD) method [116,144]. The results indicated that SiO_2 coating passivated the external BAS of HZSM-5 and successfully inhibited the alkylation of BTEX aromatics. In addition, the content of SiO_2 has significant impacts on BTEX aromatic selectivity, which can be controlled by adjusting the number of silanization cycles. After one silanization cycle, the BTEX aromatics significantly increased from 5% to 22.8%. However, on the contrary, over silanization (three cycles) resulted in pore blockage and subsequently hindered the diffusion of reaction intermediates into the micropores and inhibited the formation of BTEX aromatics. Therefore, a suitable SiO_2 coating content is crucial to promote the BTEX formation of aromatics.

3.3. Effect of the Reaction Conditions on the Catalytic Performance

For hydrogenation of CO_2 to aromatics, reaction conditions, including the reaction temperature, reaction pressure, space velocity, H_2/CO_2 ratio, and the mass ratio of different active components and mixing mode, significantly affect the catalytic performances (CO_2 conversion, CO selectivity, aromatic selectivity, BTEX selectivity, etc.). The specific content will be introduced below in detail.

3.3.1. Reaction Temperature

In general, hydrogenation of CO_2 to aromatics has a proper range of reaction temperatures. That is, too low and too high temperatures are not preferred [111]. More specifically, too low temperature is not conducive to CO_2 activation [145], whereas too high temperature may result in the hydrocracking of long-chain hydrocarbons to light paraffins. For example, Song et al. investigated effects of the reaction temperature on the CO_2 conversion and product distribution over 6.25Cu-Fe_2O_3/HZSM-5-c catalysts [115]. As shown in Figure 16a, when the reaction temperature increased from 280 °C to 320 °C, the aromatic selectivity increased by 32.46%, whereas as the temperature further increased to 360 °C, the aromatic

selectivity decreased by 27.61%, with an increase in CH_4 and C_2^0–C_4^0 selectivity of 10 and 16%, respectively. Therefore, a suitable reaction temperature is favorable for improving the product distribution.

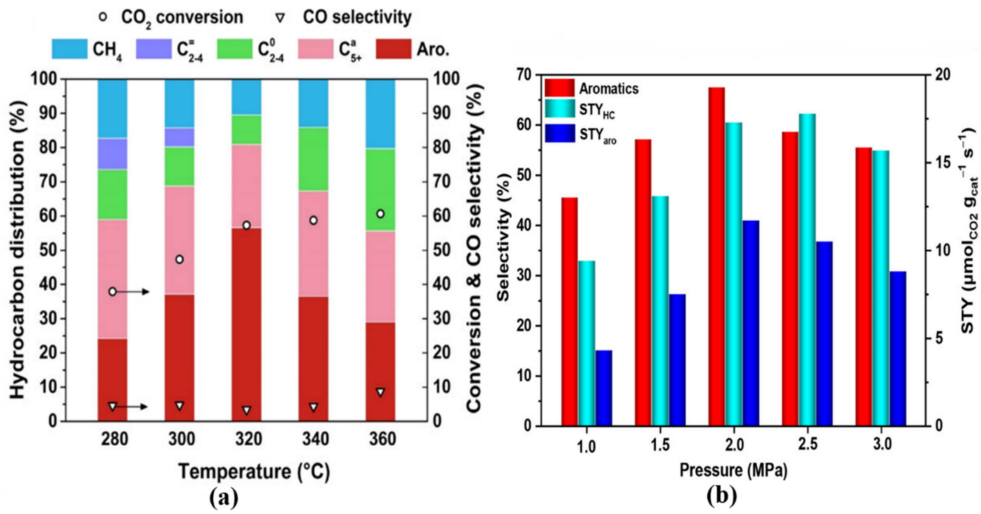

Figure 16. (**a**) Effects of the reaction temperature on the catalytic performance over 6.25Cu-Fe_2O_3/HZSM-5-c catalysts. Reaction conditions: 320 °C, 3.0 MPa, GHSV = 1000 mL·g_{cat}^{-1}·h^{-1}, $H_2/CO_2/N_2$ = 72/24/4, 2 g tandem catalysts. Reprinted with permission from Song et al. [115]. Copyright (2020) American Chemical Society. (**b**) Effects of the reaction pressure on the aromatic selectivity, STY_{HC}, and STY_{aro} over the FeK1.5/HSG | HZSM-5(50) catalysts. Other reaction conditions: 340 °C, H_2/CO_2 = 3, 150 mg of FeK1.5/HSG and 150 mg of HZSM-5(50), TOS = 24 h. Reprinted with permission from Wang et al. [112]. Copyright (2019) American Chemical Society.

3.3.2. Reaction Pressure

As mentioned above, during the hydrogenation of CO_2 to aromatics, the olefin intermediates formed on Fe-based catalysts diffuse to the pores of HZSM-5, which are subsequently converted to aromatics by oligomerization, cyclization, dehydrogenation, and aromatization [104]. During the process of aromatization, the oligomerization and cyclization reactions decrease in moles, whereas the dehydrogenation reaction increases in moles. Therefore, the effect of the reaction pressure on the hydrogenation of CO_2 to aromatics is rather complex [146]. For example, Wang et al. prepared FeK1.5/HSG | HZSM-5(50) catalysts and investigated the effects of pressure on the aromatic selectivity and space time yield of the aromatics (STY_{aro}) [53]. As shown in Figure 16b, the aromatic selectivity and STY_{aro} increased significantly by 22 and 7.4% when the pressure increased from 1.0 MPa to 2.0 MPa. It can be explained that the increase in pressure benefits the oligomerization and cyclization reactions, therefore promoting the formation of aromatics. However, on the contrary, as the pressure further increased to 3 MPa, aromatic selectivity and STY_{aro} decreased by 12 and 1.9%. Generally, dehydrogenation is a rate-limiting step during the process of olefin aromatization [147]. Therefore, too high pressure is not conducive to dehydrogenation and the formation of aromatics, indicating that a suitable pressure is important for improving aromatic selectivity and STY_{aro}.

3.3.3. Space Velocity

In addition to the reaction temperature and pressure, space velocity is also a vital factor, which determines the contact time between reactants and catalysts [128]. Sibi et al. prepared a Na-$FeAlO_x$/Zn-HZSM-5(12.5)@SiO_2 catalyst and studied the effects of space velocity on aromatics and BTEX selectivity in detail [116]. When the space velocity increased from 2000 mL·g_{cat}^{-1}·h^{-1} to 4000 mL·g_{cat}^{-1}·h^{-1}, the aromatic and BTEX selectivity increased by 5% and 6%, respectively, which is probably because a long residence time results in the secondary hydrogenation of olefins. However, when the space velocity continued to

increase to 6000 mL·g_{cat}^{-1}·h^{-1}, the aromatic and BTEX selectivity decreased by 33.8 and 18.7%, respectively. It can be explained by the fact that the reaction intermediates formed at the Fe-based active sites cannot effectively diffuse into the pores of HZSM-5 in time due to the short residence time. Therefore, a moderate space velocity is essential for improving aromatic and BTEX selectivity.

3.3.4. H_2/CO_2 Ratio

As mentioned above, the addition of active H_2 benefits CO_2 activation and its subsequent conversion and affects the secondary hydrogenation of olefins [105]. As shown in Figure 17, as the H_2/CO_2 ratio increased from 2 to 6, the CO_2 conversion increased by 30% and the CO selectivity decreased by 7.5% over the $ZnFeO_x$-4.25Na/S-HZSM-5 catalyst. This is because abundant H_2 promotes the hydrogenation of CO_2 reactants and/or CO intermediates [106], but a H_2/CO_2 ratio that is too high has an obvious effect on aromatic selectivity. More specially, increasing the H_2/CO_2 ratio from 2 to 6 resulted in a decrease in aromatic selectivity from 67.2% to 47.4%, which is due to the secondary hydrogenation of olefins under high H_2 pressure [60]. Therefore, an appropriate H_2/CO_2 ratio is important to balance the activation capacity of CO_2 and product selectivity.

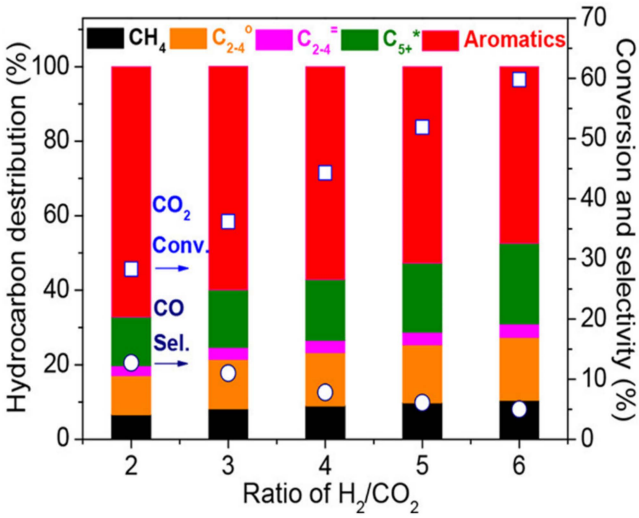

Figure 17. The effect of the H_2/CO_2 ratio on the catalytic performance over $ZnFeO_x$-4.25Na/S-HZSM-5 catalysts. Reaction conditions: 320 °C, 3.0 MPa, GHSV = 4000 mL·g_{cat}^{-1}·h^{-1}. C_{5+}* means C_{5+} products except for aromatics. Reprinted with permission from Cui et al. [60]. Copyright (2019) American Chemical Society.

3.3.5. Mass Ratio and Mixing Mode of Different Active Components

The mass ratio of different active components (zeolites/Fe oxides) and mixing mode have significant effects on the catalytic performance [64,112]. For the mass ratio, a high mass ratio is favorable for improving aromatic and PX selectivity, whereas too high mass ratios may result in isomerization and alkylation of PX. Gao et al. prepared a 2.83Na-FeMn (90/10)/HZSM-5@S1-S catalyst and studied the effects of different mass ratios on the aromatic and PX selectivity. When the mass ratio increased from 1 to 2, the aromatic and PX selectivity increased by 7.7 and 3.5%, respectively, while, as the mass ratio further increased to 3, the PX selectivity decreased by 0.6% [117]. Therefore, an appropriate mass ratio can effectively promote the generation of high-value aromatics.

For mixing mode (i.e., powder-mixing, granule-mixing, granule-mixing with quartz sand, and dual bed modes) [148,149], as shown in Figure 18, the 6.25Cu-Fe_2O_3/HZSM-5-c tandem catalyst in the granule-mixing mode showed high CO_2 conversion (57.3%) and aromatic selectivity (56.61%), whereas the powder-mixing mode had relatively lower CO_2 conversion (44%) and aromatic selectivity (30%). This may be due to the strong interaction between the acid sites of HZSM-5 and the active sites of the 6.25Cu-Fe_2O_3 surface for the

powder-mixing mode. More specially, the acid sites of HZSM-5 poison the alkali sites on the 6.25Cu-Fe_2O_3 surface, reducing the surface basicity and acidity of the 6.25Cu-Fe_2O_3 and HZSM-5, respectively, therefore suppressing CO_2 hydrogenation and olefin aromatization [115,150]. In addition, a further increase in the distance between the two active components by the dual bed mixing mode led to the deteriorated catalytic performance with CO_2 conversion (37%) and aromatic selectivity (32%). This can be attributed to the distance that hinders the intermediate transfer and weakens the thermodynamical driving force. Therefore, an appropriate mixing mode of Fe-based catalysts and HZSM-5 can exert effective synergistic effects, which contribute to improving the CO_2 conversion and aromatic selectivity [148].

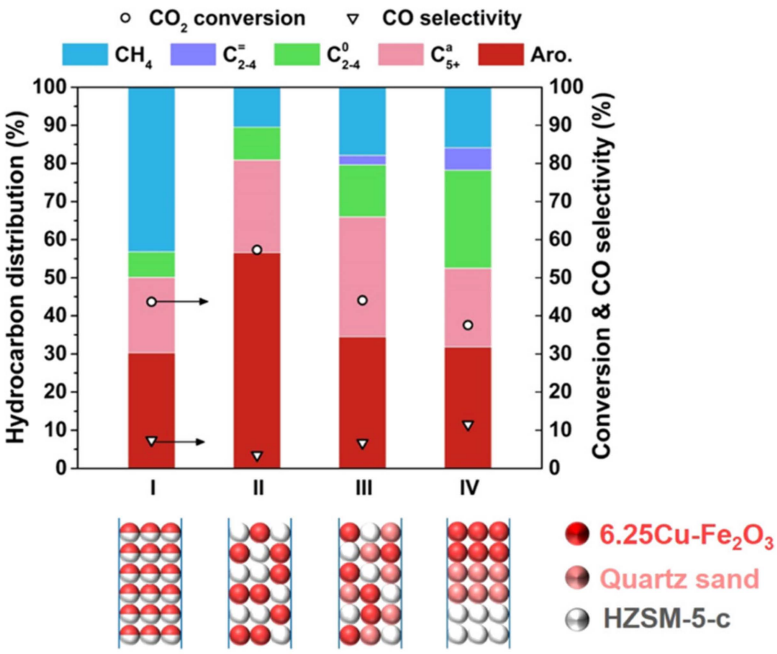

Figure 18. Effects of different mixing modes of 6.25Cu-Fe_2O_3/HZSM-5-c tandem catalysts on catalytic performance. I: Powder-mixing, II: Granule-mixing, III: Granule-mixing with quartz sand, IV: Dual bed. Reaction conditions: 320 °C, 3.0 MPa, GHSV = 1000 mL·g_{cat}^{-1}·h^{-1}, $H_2/CO_2/N_2$ = 72/24/4, 2 g tandem catalysts. Reprinted with permission from Song et al. [115]. Copyright (2020) American Chemical Society.

4. Reaction Mechanism

4.1. Mechanistic Study of the Hydrogenation of CO_2 to Liquid Fuels

The relationship between active sites and mechanisms remains controversial despite that many excellent catalysts have been developed for the hydrogenation of CO_2 to liquid fuels. According to the most-accepted reaction mechanism [151,152], the mechanism for RWGS can be identified as either the decomposition of HOCO* species or the direct cleavage of C=O bonds to generate CO* [153]. During the FTS process, the main steps include the formation of CH_x* monomers (x = 0–3) with hydrogen-assisted insertion into dissociated CO* [154], the initiation of chain growth through the coupling of CH_x*, and the termination of chain growth through further hydrogenation, dehydrogenation, or CO insertion (Figure 19), leading to the formation of paraffins, olefins, and oxygenates.

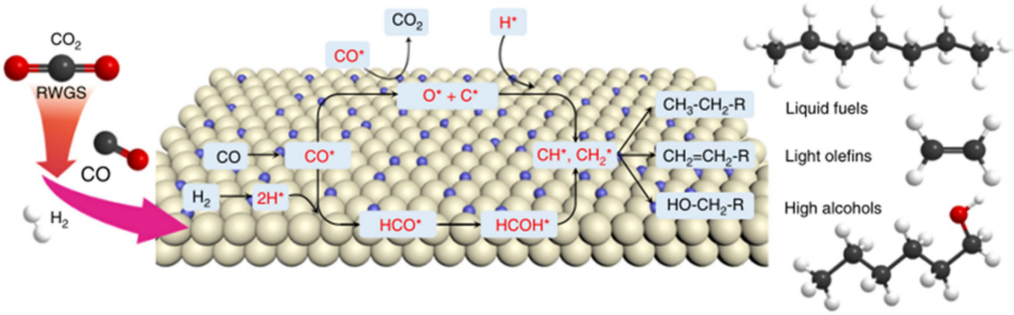

Figure 19. Scheme of CO_2-modified FTS-based catalytic mechanism. Reprinted with permission from Ye et al. [155]. Copyright (2019) Springer Nature.

The formation of CH_x* monomers and the growth of the carbon chain [156] directly affect the hydrogenation of CO_2 to liquid fuels. Firstly, the formation of CH_x* monomers is related to the composition of catalysts. For example, Nie et al. studied CO_2 hydrogenation on the surfaces of pure Fe and bimetallic Fe-Cu catalysts with DFT calculations and identified favorable pathways through the HCOO* intermediates (CO_2* → HCOO* → HCOOH* → HCO* → HCOH* → CH*) rather than the formation of CO* (CO_2* → CO* → HCO* → HCOH* → CH*). This is attributed to the bimetallic synergetic effects of Fe-Cu, in which the addition of Cu reduces the barrier for C–C coupling and facilitates carbon chain growth (Figure 20) [157]. Therefore, the addition of secondary metals not only enhances CO_2 conversion but also changes the pathway of CO_2 hydrogenation.

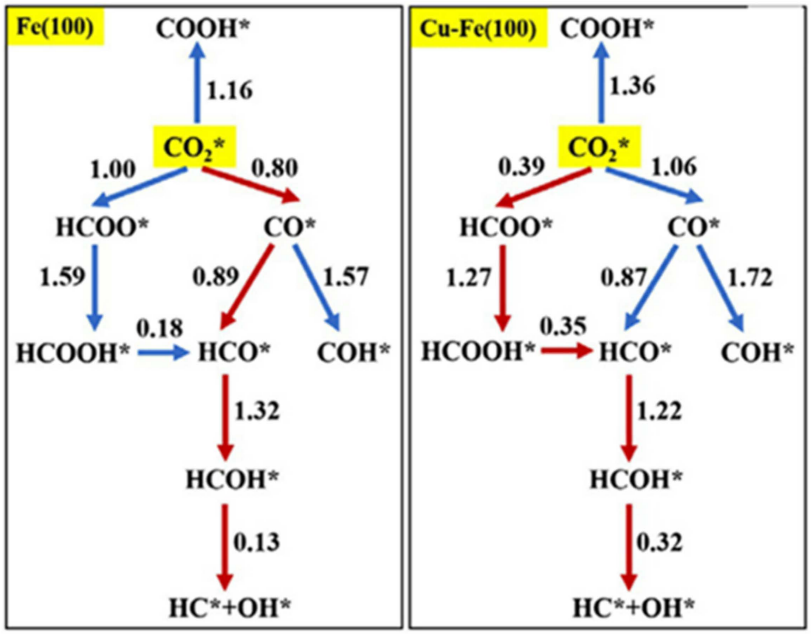

Figure 20. Reaction networks examined to identify energetically favorable C_1 species from CO_2 hydrogenation on the Fe (100) and Cu-Fe (100) surface. Activation barriers are given in eV (the networks connected with red arrows represent the preferred path for CO_2 conversion to CH*). Reprinted with permission from Nie et al. [157]. Copyright (2017) American Chemical Society.

Secondly, two possible mechanisms are proposed for the carbon chain growth based on the FTS reaction [158]: the "carbide" mechanism [159] and the "CO insertion" mechanism [160,161] (Figure 21). The "carbide" mechanism involves the formation of CH_x* species through CO* dissociation and subsequent chain growth by CH_x* species insertion. First, the CH_x* species produced from CO* dissociation initiate the entire reaction, and then carbon chain growth is achieved by the insertion of subsequent CH_x* species, for which the

CH* and CH_2* are identified as key CH_x* species, whereas the "CO insertion" mechanism realizes carbon chain growth by the direct insertion of undissociated CO into CH_x* species. Herein, CH_x* species initiate the whole reaction, and subsequent CO* is inserted into the generated CH_x* species, and then the initial C_2H_x* species are formed through the C–O bonds cleavage of C_2 oxygenic intermediates, and further carbon chain growth continues by continuously inserting CO* into the C_nH_x* species [160,162]. According to DFT calculations, Fe-Cu bimetallic catalysts generally follow the "carbide" mechanism [157], and Co-based catalysts generally follow the "CO insertion" mechanism [163,164]. Therefore, both the "carbide" and "CO insertion" mechanisms are applicable to the hydrogenation of CO_2 to liquid fuels, which depends on the types and properties of the used catalysts.

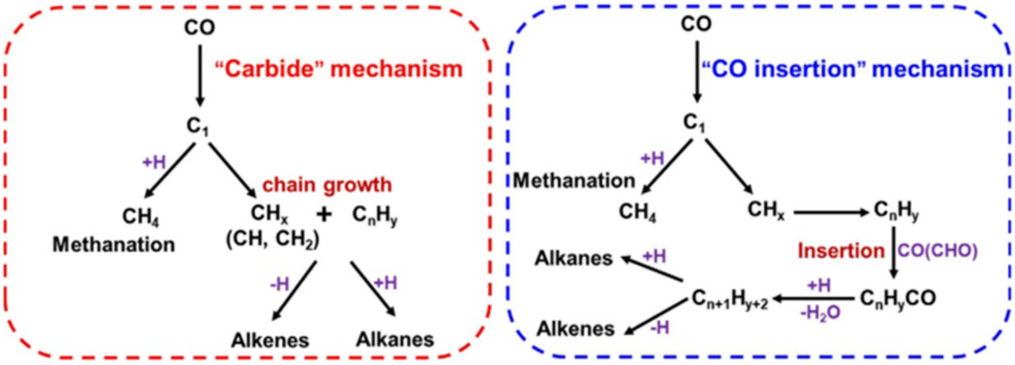

Figure 21. Schematic illustration of the "carbide" and "CO insertion" mechanisms proposed in CO-FTS for hydrocarbon synthesis. Reprinted with permission from Nie et al. [20]. Copyright (2019) published Elsevier. Reprinted with permission from van Santen et al. [158]. Copyright (2013) The Royal Society of Chemistry.

4.2. Mechanistic Study of the Hydrogenation of CO_2 to Aromatics

The hydrogenation of CO_2 to aromatics via the FTS route mainly uses tandem catalysts composed of Fe-based active components and HZSM-5. In general, Fe_3O_4 and Fe_xC_y are considered active sites for RWGS and FTS, respectively, while aromatization of olefin intermediates mainly occurs on the acid sites of HZSM-5. For example, Gascon et al. [118] proposed a reaction pathway for the hydrogenation of CO_2 to aromatics over Fe_2O_3@KO_2/HZSM-5 tandem catalysts, as illustrated in (Figure 22). In more detail, as shown in Figure 22a, CO_2 is initially converted to CO via RWGS over the Fe_3O_4 active sites. Next, a portion of as-formed CO is directly converted into hydrocarbons over the Fe_xC_y active sites, and the remaining portion of CO diffuses into the confined pores of HZSM-5 to form surface-formate species, which are subsequently converted to surface-methoxy species (SMS) in situ via hydrogenation [165]. Then, SMS is further converted into ethylene via a series of reactions including CO insertion, hydrogenation, and deprotonation as seen in Figure 22b. Finally, the olefin intermediates formed via the aforementioned two pathways are converted into aromatics by oligomerization, cyclization, hydrogen transfer, and aromatization on HZSM-5 as shown (Figure 22c).

Sibi et al. used situ operando diffuse reflectance infrared Fourier-transform spectroscopy (DRIFTS) experiments to obtain a plausible reaction for the formation of ethylene species over HZSM-5(12.5) zeolite [116]. As the pressure increased from 1 to 3 MPa, CO_2-adsorbed species (b-CO_3^{2-} [166], HCO_3^- [167,168], and –OH), L-CO, water, and CH_4 were observed. Moreover, peaks associated with ethylene vibrations (3125 cm^{-1}, 3079 cm^{-1}, 2989 cm^{-1}, 2048 cm^{-1}, 1889 cm^{-1}, and 1445 cm^{-1}) were also observed. This suggests that the surface –OH groups of pristine H-ZSM5(12.5) promote the RWGS and C–C coupling reactions to a certain degree. In detail, the silanol groups and the extra framework aluminum (EFAL) species could be regarded as the adsorption sites of CO_2. Over the EFAL site, bicarbonate species can be converted to formate and dissociate to generate CO* and *OH. Then, the hydrogenation of CO* with the hydrogen from the adsorbed H species in

HZSM-5(12.5) produces CH_x species, and subsequent C–C coupling could finally produce ethylene. However, Wang et.al. reported that the synergistic effects between BAS and LAS also play a vital role in enhancing the formation of aromatics. Taking the aromatization of cyclohexene as an example [113], the cyclohexene is able to form carbenium ions on the LAS by dehydrogenation. Then, the hydride combines with the acidic proton in the BAS, releasing H_2. Meanwhile, the cyclic carbocation undergoes further dehydrogenation, leading to the formation of cyclohexene and the recovery of BAS. After this process is repeated, aromatics are finally produced.

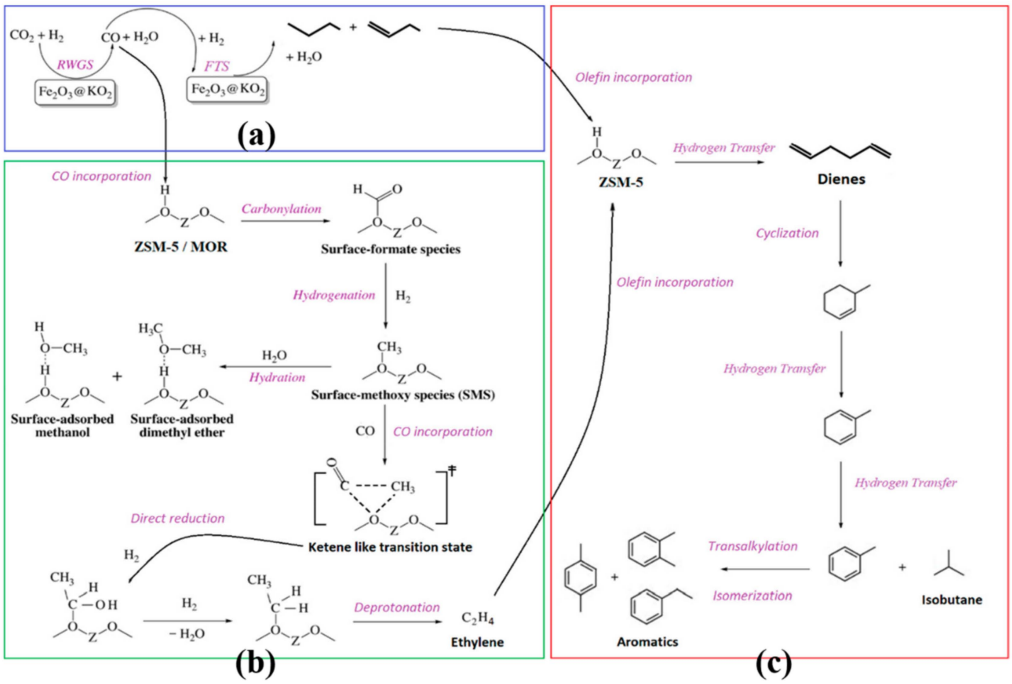

Figure 22. Proposed reaction pathways of $Fe_2O_3@KO_2$/zeolite catalyst hydrogenation of CO_2 to light olefins and aromatics. (**a**) CO_2 hydrogenation pathway on the stand-alone $Fe_2O_3@KO_2$ catalysts. (**b**) CO incorporation pathway on HZSM-5. (**c**) Aromatization pathway on HZSM-5. Reprinted with permission from Ramirez et al. [118]. Copyright (2019) American Chemical Society.

In addition, Song et al. found that the synthesis of aromatics involving dehydrogenation and cyclization of light olefins resulted in abundant H species [169]. If these H species cannot be consumed or diffuse out immediately, then the high concentration of H present in the system will inhibit the aromatization of olefins [170]. These authors proposed a "H recycling" mechanism, as shown in Figure 23 [115], in which the H species formed during the aromatization of olefins on the acid sites of HZSM-5 can diffuse to the surface of the Fe active sites and react with the absorbed CO_2 on the oxygen vacancy. In other words, Fe active species act as "H acceptors" to hold H species that originate from HZSM-5. Meanwhile, CO_2 acts as a "H consumer" to promote the formation and subsequent aromatization of olefins.

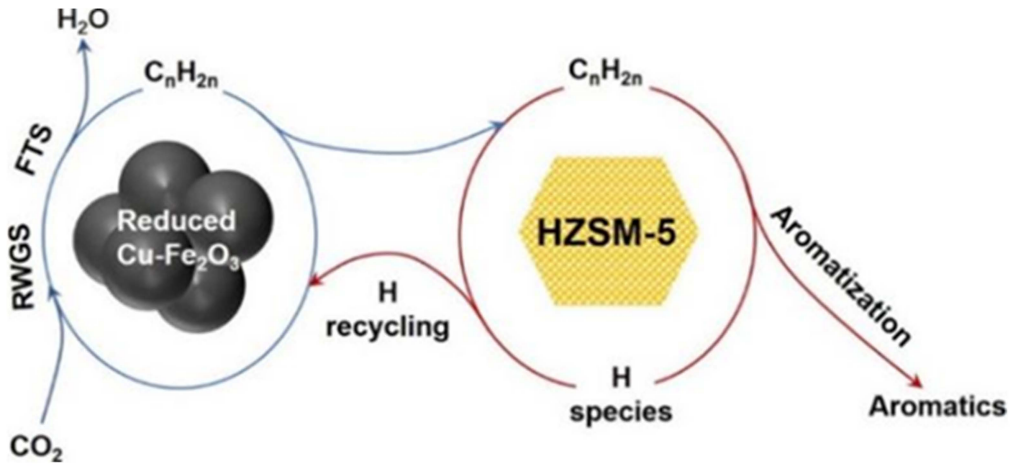

Figure 23. Schematic illustration of the "H recycling" mechanism for CO_2 hydrogenation to aromatics between oxide and zeolite. Reprinted with permission from Song et al. [115]. Copyright (2020) American Chemical Society.

5. Conclusions and Perspective

To mitigate climate change and achieve carbon neutrality, the hydrogenation of CO_2 to liquid fuels and aromatics is considered to be a promising and sustainable technology that can effectively reduce CO_2 emissions and convert waste CO_2 into high value-added products. In this review, we have critically and comprehensively summarized the recent research progress of the development of efficient Fe-based catalysts for the hydrogenation of CO_2 to liquid fuels and aromatics via the FTS route.

For the hydrogenation of CO_2 to liquid fuels, the alkali promoters, secondary metals, catalyst supports, and preparation methods have significant effects on the catalytic performances. In more detail, alkali promoters can effectively enhance the capacity of carbon chain growth and improve olefin selectivity. The addition of secondary metals can form specific bimetallic structures, which promote the formation and stability of Fe active species, thus facilitating carbon chain growth via C–C coupling. Catalyst supports with a high specific surface area generally benefit the dispersion of Fe species; however, the interaction between Fe active components and supports should be properly regulated because too strong a metal-support interaction is not conducive to the catalytic performance. The preparation methods can effectively regulate the physical properties of the catalysts that are closely associated with the efficient production of liquid fuels. In addition, tandem catalysts using the acidity and porous properties of zeolites can further enhance the selectivity and octane number of liquid fuels.

The formation and subsequent aromatization of olefin intermediates are critical for the hydrogenation of CO_2 to aromatics over the FeO_x/zeolites tandem catalysts, where zeolites play a key role in aromatization. Herein, HZSM-5 is preferred due to the suitable surface acidity and pore structure; however, it is easy to form heavy aromatics and deactivate due to carbon deposition. To address these issues, a series of strategies, such as alkali treatment, cationic modification, and SiO_2 coating, have been applied to regulate the surface acidity and pore structure of HZSM-5. More specially, alkali treatment regulates the BAS and LAS density by redistributing the framework of Al and generates a hierarchical pore structure, which promotes the formation of aromatics and catalyst stability. Moreover, cationic modification (Zn, P, Ga, etc.) can increase the LAS density, which facilitates direct dehydrogenation, therefore promoting the formation of olefin intermediates and targeted aromatics. In addition, SiO_2 coating passivates the external BAS of HZSM-5 and effectively inhibits the alkylation and isomerization of aromatics.

However, there are a variety of challenges in the preparation of catalysts for CO_2 hydrogenation to liquid fuels and aromatics. We should pay sufficient attention to catalyst design in order to achieve a balance of synergistic effects between alkali promoters and

secondary metals towards liquid fuel synthesis or Fe-based active components and the acid sites of zeolites towards aromatic synthesis through the combination of preparation methods from multiple fields and disciplines. Apart from developing efficient catalysts for suitable reaction conditions, we should also focus on the optimization or design of new reactors to facilitate the CO_2 conversion and remove the by-product, i.e., water [11]. For example, the membrane reactor with selective permeation membranes can selectively filter water [171], thereby breaking the reaction equilibrium and promoting the forward process of CO_2 hydrogenation, thus greatly improving the CO_2 conversion and long-chain hydrocarbon (i.e., liquid fuels and aromatics) selectivity. In addition, with the development of computational tools relevant for catalysis, it will become an important research direction to further study the reaction mechanisms combining DFT calculation results and existing experimental data and to predict the relationship between the properties (the particle sizes and distribution of Fe-based catalyst active components, the pore sizes of supports) and catalytic performances (activity, selectivity, and stability) of catalysts. In addition to the various challenges discussed above, H_2 production technologies have also received considerable attention. Generally, water electrolysis using renewable energies is considered a potential and sustainable technology to produce green H_2, whereas the technology still faces challenges in terms of technical maturity and cost. However, with the development of efficient water electrolysis technologies and large-scale deployment of renewable energies, it is expected that CO_2 hydrogenation technologies for value-added chemicals and fuels using green H_2 will become more feasible and competitive.

Author Contributions: Conceptualization, Q.W. and K.H.; methodology, R.G.; validation, L.Z., L.W.; formal analysis, R.G.; investigation, Q.W.; resources, C.Z.; writing—original draft preparation, R.G.; writing—review and editing, C.Z.; visualization, K.H.; supervision, C.Z.; project administration, C.Z.; funding acquisition, C.Z. All authors have read and agreed to the published version of the manuscript.

Funding: This research was supported by the "Next Generation Carbon Upcycling Project" (Project No. 2017M1A2A2043133) through the National Research Foundation (NRF) funded by the Ministry of Science and ICT, Republic of Korea. We also appreciate the Natural Science Foundation of Jiangsu Province (BK20200694, 20KJB530002, 21KJB480014), and the open program of the State Key Laboratory of High-efficiency Utilization of Coal and Green Chemical Engineering (2021-K32).

Institutional Review Board Statement: Not applicable.

Informed Consent Statement: Not applicable.

Data Availability Statement: All the data are presented in the manuscript.

Conflicts of Interest: The authors declare that they have no known competing financial interests or personal relationships that could have appeared to influence the work reported in this paper.

References

1. Doney, S.C.; Fabry, V.J.; Feely, R.A.; Kleypas, J.A. Ocean Acidification: The Other CO_2 Problem. *Annu. Rev. Mar. Sci.* **2009**, *1*, 169–192. [CrossRef] [PubMed]
2. Solomon, S.; Plattner, G.K.; Knutti, R.; Friedlingstein, P. Irreversible climate change due to carbon dioxide emissions. *Proc. Natl. Acad. Sci. USA* **2009**, *106*, 1704–1709. [CrossRef] [PubMed]
3. IEA. World CO_2 emissions from fuel combustion by region, 1971–2018. In *CO_2 Emissions from Fuel Combustion*; IEA: Paris, France, 2020. Available online: https://www.iea.org/data-and-statistics/charts/world-CO2-emissions-from-fuel-combustion-by-region-1971-2018 (accessed on 14 March 2022).
4. Davis, S.J.; Caldeira, K.; Matthews, H.D. Future CO_2 emissions and climate change from existing energy infrastructure. *Science* **2010**, *329*, 1330–1333. [CrossRef]
5. Rogelj, J.; den Elzen, M.; Höhne, N.; Fransen, T.; Fekete, H.; Winkler, H.; Schaeffer, R.; Sha, F.; Riahi, K.; Meinshausen, M. Paris Agreement climate proposals need a boost to keep warming well below 2 °C. *Nature* **2016**, *534*, 631–639. [CrossRef] [PubMed]
6. Prieto, G. Carbon Dioxide Hydrogenation into Higher Hydrocarbons and Oxygenates: Thermodynamic and Kinetic Bounds and Progress with Heterogeneous and Homogeneous Catalysis. *ChemSusChem* **2017**, *10*, 1056–1070. [CrossRef] [PubMed]
7. Galadima, A.; Muraza, O. Catalytic thermal conversion of CO_2 into fuels: Perspective and challenges. *Renew. Sustain. Energy Rev.* **2019**, *115*, 109333. [CrossRef]

8. Daza, Y.A.; Kuhn, J.N. CO_2 conversion by reverse water gas shift catalysis: Comparison of catalysts, mechanisms and their consequences for CO_2 conversion to liquid fuels. *RSC Adv.* **2016**, *6*, 49675–49691. [CrossRef]
9. Dorner, R.W.; Hardy, D.R.; Williams, F.W.; Willauer, H.D. Heterogeneous catalytic CO_2 conversion to value-added hydrocarbons. *Energy Environ. Sci.* **2010**, *3*, 884–890. [CrossRef]
10. Saeidi, S.; Amin, N.A.S.; Rahimpour, M.R. Hydrogenation of CO_2 to value-added products-A review and potential future developments. *J. CO2 Util.* **2014**, *5*, 66–81. [CrossRef]
11. Gao, P.; Zhang, L.; Li, S.; Zhou, Z.; Sun, Y. Novel Heterogeneous Catalysts for CO_2 Hydrogenation to Liquid Fuels. *ACS Cent. Sci.* **2020**, *6*, 1657–1670. [CrossRef]
12. Du, G.; Lim, S.; Yang, Y.; Wang, C.; Pfefferle, L.; Haller, G.L. Methanation of carbon dioxide on Ni-incorporated MCM-41 catalysts: The influence of catalyst pretreatment and study of steady-state reaction. *J. Catal.* **2007**, *249*, 370–379. [CrossRef]
13. Janke, C.; Duyar, M.S.; Hoskins, M.; Farrauto, R. Catalytic and adsorption studies for the hydrogenation of CO_2 to methane. *Appl. Catal. B Environ.* **2014**, *152–153*, 184–191. [CrossRef]
14. Perkas, N.; Amirian, G.; Zhong, Z.; Teo, J.; Gofer, Y.; Gedanken, A. Methanation of Carbon Dioxide on Ni Catalysts on Mesoporous ZrO_2 Doped with Rare Earth Oxides. *Catal. Lett.* **2009**, *130*, 455–462. [CrossRef]
15. Zhong, H.; Yao, G.; Cui, X.; Yan, P.; Wang, X.; Jin, F. Selective conversion of carbon dioxide into methane with a 98% yield on an in situ formed Ni nanoparticle catalyst in water. *Chem. Eng. J.* **2019**, *357*, 421–427. [CrossRef]
16. Liu, J.; Zhang, A.; Jiang, X.; Liu, M.; Zhu, J.; Song, C.; Guo, X. Direct Transformation of Carbon Dioxide to Value-Added Hydrocarbons by Physical Mixtures of Fe_5C_2 and K-Modified Al_2O_3. *Ind. Eng. Chem. Res.* **2018**, *57*, 9120–9126. [CrossRef]
17. Xu, Z.; McNamara, N.D.; Neumann, G.T.; Schneider, W.F.; Hicks, J.C. Catalytic Hydrogenation of CO_2 to Formic Acid with Silica-Tethered Iridium Catalysts. *ChemCatChem* **2013**, *5*, 1769–1771. [CrossRef]
18. Hao, C.; Wang, S.; Li, M.; Kang, L.; Ma, X. Hydrogenation of CO_2 to formic acid on supported ruthenium catalysts. *Catal. Today* **2011**, *160*, 184–190. [CrossRef]
19. Mori, K.; Taga, T.; Yamashita, H. Isolated Single-Atomic Ru Catalyst Bound on a Layered Double Hydroxide for Hydrogenation of CO_2 to Formic Acid. *ACS Catal.* **2017**, *7*, 3147–3151. [CrossRef]
20. Nie, X.; Li, W.; Jiang, X.; Guo, X.; Song, C. Recent advances in catalytic CO_2 hydrogenation to alcohols and hydrocarbons. *Adv. Catal.* **2019**, *65*, 121–233.
21. Nezam, I.; Zhou, W.; Gusmão, G.S.; Realff, M.J.; Wang, Y.; Medford, A.J.; Jones, C.W. Direct aromatization of CO_2 via combined CO_2 hydrogenation and zeolite-based acid catalysis. *J. CO2 Util.* **2021**, *45*, 101405. [CrossRef]
22. Yang, H.; Zhang, C.; Gao, P.; Wang, H.; Li, X.; Zhong, L.; Wei, W.; Sun, Y. A review of the catalytic hydrogenation of carbon dioxide into value-added hydrocarbons. *Catal. Sci. Technol.* **2017**, *7*, 4580–4598. [CrossRef]
23. Martinez-Espin, J.S.; Mortén, M.; Janssens, T.V.W.; Svelle, S.; Beato, P.; Olsbye, U. New insights into catalyst deactivation and product distribution of zeolites in the methanol-to-hydrocarbons (MTH) reaction with methanol and dimethyl ether feeds. *Catal. Sci. Technol.* **2017**, *7*, 2700–2716. [CrossRef]
24. Wei, J.; Yao, R.; Han, Y.; Ge, Q.; Sun, J. Towards the development of the emerging process of CO_2 heterogenous hydrogenation into high-value unsaturated heavy hydrocarbons. *Chem. Soc. Rev.* **2021**. [CrossRef] [PubMed]
25. Kangvansura, P.; Chew, L.M.; Saengsui, W.; Santawaja, P.; Poo-arporn, Y.; Muhler, M.; Schulz, H.; Worayingyong, A. Product distribution of CO_2 hydrogenation by K- and Mn-promoted Fe catalysts supported on N-functionalized carbon nanotubes. *Catal. Today* **2016**, *275*, 59–65. [CrossRef]
26. Chew, L.M.; Kangvansura, P.; Ruland, H.; Schulte, H.J.; Somsen, C.; Xia, W.; Eggeler, G.; Worayingyong, A.; Muhler, M. Effect of nitrogen doping on the reducibility, activity and selectivity of carbon nanotube-supported iron catalysts applied in CO_2 hydrogenation. *Appl. Catal. A Gen.* **2014**, *482*, 163–170. [CrossRef]
27. Cui, M.; Qian, Q.; Zhang, J.; Wang, Y.; Asare Bediako, B.B.; Liu, H.; Han, B. Liquid fuel synthesis via CO_2 hydrogenation by coupling homogeneous and heterogeneous catalysis. *Chem* **2021**, *7*, 726–737. [CrossRef]
28. Zhang, L.; Dang, Y.; Zhou, X.; Gao, P.; Petrus van Bavel, A.; Wang, H.; Li, S.; Shi, L.; Yang, Y.; Vovk, E.I.; et al. Direct conversion of CO_2 to a jet fuel over CoFe alloy catalysts. *Innovation* **2021**, *2*, 100170. [CrossRef]
29. Jo, H.; Khan, M.K.; Irshad, M.; Arshad, M.W.; Kim, S.K.; Kim, J. Unraveling the role of cobalt in the direct conversion of CO_2 to high-yield liquid fuels and lube base oil. *Appl. Catal. B Environ.* **2022**, *305*, 121041. [CrossRef]
30. Shi, Z.; Yang, H.; Gao, P.; Chen, X.; Liu, H.; Zhong, L.; Wang, H.; Wei, W.; Sun, Y. Effect of alkali metals on the performance of $CoCu/TiO_2$ catalysts for CO_2 hydrogenation to long-chain hydrocarbons. *Chin. J. Catal.* **2018**, *39*, 1294–1302. [CrossRef]
31. Shi, Z.; Yang, H.; Gao, P.; Li, X.; Zhong, L.; Wang, H.; Liu, H.; Wei, W.; Sun, Y. Direct conversion of CO_2 to long-chain hydrocarbon fuels over K-promoted $CoCu/TiO_2$ catalysts. *Catal. Today* **2018**, *311*, 65–73. [CrossRef]
32. Tarasov, A.L.; Isaeva, V.I.; Tkachenko, O.P.; Chernyshev, V.V.; Kustov, L.M. Conversion of CO_2 into liquid hydrocarbons in the presence of a Co-containing catalyst based on the microporous metal-organic framework MIL-53(Al). *Fuel Processing Technol.* **2018**, *176*, 101–106. [CrossRef]
33. He, Z.; Cui, M.; Qian, Q.; Zhang, J.; Han, B. Synthesis of liquid fuel via direct hydrogenation of CO_2. *Proc. Natl. Acad. Sci. USA* **2019**, *116*, 12654–12659. [CrossRef] [PubMed]
34. Calizzi, M.; Mutschler, R.; Patelli, N.; Migliori, A.; Zhao, K.; Pasquini, L.; Zuettel, A. CO_2 Hydrogenation over Unsupported Fe-Co Nanoalloy Catalysts. *Nanomaterials* **2020**, *10*, 1360. [CrossRef]

35. Bae, J.W.; Park, S.-J.; Kang, S.-H.; Lee, Y.-J.; Jun, K.-W.; Rhee, Y.-W. Effect of Cu content on the bifunctional Fischer–Tropsch Fe–Cu–K/ZSM5 catalyst. *J. Ind. Eng. Chem.* **2009**, *15*, 798–802. [CrossRef]
36. Hwang, S.-M.; Han, S.J.; Park, H.-G.; Lee, H.; An, K.; Jun, K.-W.; Kim, S.K. Atomically Alloyed Fe–Co Catalyst Derived from a N-Coordinated Co Single-Atom Structure for CO_2 Hydrogenation. *ACS Catal.* **2021**, *11*, 2267–2278. [CrossRef]
37. Satthawong, R.; Koizumi, N.; Song, C.; Prasassarakich, P. Bimetallic Fe–Co catalysts for CO_2 hydrogenation to higher hydrocarbons. *J. CO2 Util.* **2013**, *3–4*, 102–106. [CrossRef]
38. Zhang, Z.; Yin, H.; Yu, G.; He, S.; Kang, J.; Liu, Z.; Cheng, K.; Zhang, Q.; Wang, Y. Selective hydrogenation of CO_2 and CO into olefins over Sodium- and Zinc-Promoted iron carbide catalysts. *J. Catal.* **2021**, *395*, 350–361. [CrossRef]
39. Zhang, J.; Lu, S.; Su, X.; Fan, S.; Ma, Q.; Zhao, T. Selective formation of light olefins from CO_2 hydrogenation over Fe–Zn–K catalysts. *J. CO2 Util.* **2015**, *12*, 95–100. [CrossRef]
40. Zhang, Z.; Huang, G.; Tang, X.; Yin, H.; Kang, J.; Zhang, Q.; Wang, Y. Zn and Na promoted Fe catalysts for sustainable production of high-valued olefins by CO_2 hydrogenation. *Fuel* **2022**, *309*, 122105. [CrossRef]
41. Choi, P.H.; Jun, K.-W.; Lee, S.-J.; Choi, M.-J.; Lee, K.-W. Hydrogenation of carbon dioxide over alumina supported Fe-K catalysts. *Catal. Lett.* **1996**, *40*, 115–118. [CrossRef]
42. Albrecht, M.; Rodemerck, U.; Schneider, M.; Broering, M.; Baabe, D.; Kondratenko, E.V. Unexpectedly efficient CO_2 hydrogenation to higher hydrocarbons over non-doped Fe_2O_3. *Appl. Catal. B Environ.* **2017**, *204*, 119–126. [CrossRef]
43. Geng, S.; Jiang, F.; Xu, Y.; Liu, X. Iron-based Fischer-Tropsch synthesis for the efficient conversion of carbon dioxide into isoparaffins. *ChemCatChem* **2016**, *8*, 1303–1307. [CrossRef]
44. Wang, J.; You, Z.; Zhang, Q.; Deng, W.; Wang, Y. Synthesis of lower olefins by hydrogenation of carbon dioxide over supported iron catalysts. *Catal. Today* **2013**, *215*, 186–193. [CrossRef]
45. Xie, T.; Wang, J.; Ding, F.; Zhang, A.; Li, W.; Guo, X.; Song, C. CO_2 hydrogenation to hydrocarbons over alumina-supported iron catalyst: Effect of support pore size. *J. CO2 Util.* **2017**, *19*, 202–208. [CrossRef]
46. Boreriboon, N.; Jiang, X.; Song, C.; Prasassarakich, P. Higher Hydrocarbons Synthesis from CO_2 Hydrogenation Over K- and La-Promoted Fe-Cu/TiO_2 Catalysts. *Top. Catal.* **2018**, *61*, 1551–1562. [CrossRef]
47. Sai Prasad, P.S.; Bae, J.W.; Jun, K.-W.; Lee, K.-W. Fischer–Tropsch Synthesis by Carbon Dioxide Hydrogenation on Fe-Based Catalysts. *Catal. Surv. Asia* **2008**, *12*, 170–183. [CrossRef]
48. Hwang, S.-M.; Han, S.J.; Min, J.E.; Park, H.-G.; Jun, K.-W.; Kim, S.K. Mechanistic insights into Cu and K promoted Fe-catalyzed production of liquid hydrocarbons via CO_2 hydrogenation. *J. CO2 Util.* **2019**, *34*, 522–532. [CrossRef]
49. Khan, M.K.; Butolia, P.; Jo, H.; Irshad, M.; Han, D.; Nam, K.-W.; Kim, J. Selective Conversion of Carbon Dioxide into Liquid Hydrocarbons and Long-Chain α-Olefins over Fe-Amorphous AlOx Bifunctional Catalysts. *ACS Catal.* **2020**, *10*, 10325–10338. [CrossRef]
50. Liu, J.; Zhang, A.; Jiang, X.; Liu, M.; Sun, Y.; Song, C.; Guo, X. Selective CO_2 Hydrogenation to Hydrocarbons on Cu-Promoted Fe-Based Catalysts: Dependence on Cu-Fe Interaction. *ACS Sustain. Chem. Eng.* **2018**, *6*, 10182–10190. [CrossRef]
51. Wang, W.; Jiang, X.; Wang, X.; Song, C. Fe-Cu Bimetallic Catalysts for Selective CO_2 Hydrogenation to Olefin-Rich C_2^+ Hydrocarbons. *Ind. Eng. Chem. Res.* **2018**, *57*, 4535–4542. [CrossRef]
52. Choi, Y.H.; Jang, Y.J.; Park, H.; Kim, W.Y.; Lee, Y.H.; Choi, S.H.; Lee, J.S. Carbon dioxide Fischer-Tropsch synthesis: A new path to carbon-neutral fuels. *Appl. Catal. B Environ.* **2017**, *202*, 605–610. [CrossRef]
53. Ning, W.; Li, B.; Wang, B.; Yang, X.; Jin, Y. Enhanced Production of C_{5+} Hydrocarbons from CO_2 Hydrogenation by the Synergistic Effects of Pd and K on γ-Fe_2O_3 Catalyst. *Catal. Lett.* **2019**, *149*, 431–440. [CrossRef]
54. Ma, D.; Xu, Y.; Zhai, P.; Deng, Y.; Xie, J.; Liu, X.; Wang, S. Highly Selective Olefin Production from CO_2 Hydrogenation on Iron Catalysts: A Subtle Synergy between Manganese and Sodium Additives. *Angew. Chem.* **2020**, *132*, 21920–21928.
55. Liang, B.; Sun, T.; Ma, J.; Duan, H.; Li, L.; Yang, X.; Zhang, Y.; Su, X.; Huang, Y.; Zhang, T. Mn decorated Na/Fe catalysts for CO_2 hydrogenation to light olefins. *Catal. Sci. Technol.* **2019**, *9*, 456–464. [CrossRef]
56. Yao, B.; Xiao, T.; Makgae, O.A.; Jie, X.; Gonzalez-Cortes, S.; Guan, S.; Kirkland, A.I.; Dilworth, J.R.; Al-Megren, H.A.; Alshihri, S.M.; et al. Transforming carbon dioxide into jet fuel using an organic combustion-synthesized Fe-Mn-K catalyst. *Nat. Commun.* **2020**, *11*, 6395. [CrossRef]
57. Zhao, H.; Guo, L.; Gao, W.; Chen, F.; Wu, X.; Wang, K.; He, Y.; Zhang, P.; Yang, G.; Tsubaki, N. Multi-Promoters Regulated Iron Catalyst with Well-Matching Reverse Water-Gas Shift and Chain Propagation for Boosting CO_2 Hydrogenation. *J. CO2 Util.* **2021**, *52*, 101700. [CrossRef]
58. Jiang, F.; Liu, B.; Geng, S.; Xu, Y.; Liu, X. Hydrogenation of CO_2 into hydrocarbons: Enhanced catalytic activity over Fe-based Fischer-Tropsch catalysts. *Catal. Sci. Technol.* **2018**, *8*, 4097–4107. [CrossRef]
59. Choi, Y.H.; Ra, E.C.; Kim, E.H.; Kim, K.Y.; Jang, Y.J.; Kang, K.-N.; Choi, S.H.; Jang, J.-H.; Lee, J.S. Sodium-Containing Spinel Zinc Ferrite as a Catalyst Precursor for the Selective Synthesis of Liquid Hydrocarbon Fuels. *ChemSusChem* **2017**, *10*, 4764–4770. [CrossRef]
60. Cui, X.; Gao, P.; Li, S.; Yang, C.; Liu, Z.; Wang, H.; Zhong, L.; Sun, Y. Selective Production of Aromatics Directly from Carbon Dioxide Hydrogenation. *ACS Catal.* **2019**, *9*, 3866–3876. [CrossRef]
61. Liu, J.; Sun, Y.; Jiang, X.; Zhang, A.; Song, C.; Guo, X. Pyrolyzing ZIF-8 to N-doped porous carbon facilitated by iron and potassium for CO_2 hydrogenation to value-added hydrocarbons. *J. CO2 Util.* **2018**, *25*, 120–127. [CrossRef]

62. Liu, J.; Zhang, A.; Liu, M.; Hu, S.; Ding, F.; Song, C.; Guo, X. Fe-MOF-derived highly active catalysts for carbon dioxide hydrogenation to valuable hydrocarbons. *J. CO2 Util.* **2017**, *21*, 100–107. [CrossRef]
63. Kosol, R.; Guo, L.; Kodama, N.; Zhang, P.; Reubroycharoen, P.; Vitidsant, T.; Taguchi, A.; Abe, T.; Chen, J.; Yang, G.; et al. Iron catalysts supported on nitrogen functionalized carbon for improved CO_2 hydrogenation performance. *Catal. Commun.* **2021**, *149*, 106216. [CrossRef]
64. Guo, L.; Sun, J.; Ji, X.; Wei, J.; Wen, Z.; Yao, R.; Xu, H.; Ge, Q. Directly converting carbon dioxide to linear α-olefins on bio-promoted catalysts. *Commun. Chem.* **2018**, *1*, 11. [CrossRef]
65. Wang, S.; Wu, T.; Lin, J.; Ji, Y.; Yan, S.; Pei, Y.; Xie, S.; Zong, B.; Qiao, M. Iron–Potassium on Single-Walled Carbon Nanotubes as Efficient Catalyst for CO_2 Hydrogenation to Heavy Olefins. *ACS Catal.* **2020**, *10*, 6389–6401. [CrossRef]
66. Chernyak, S.A.; Ivanov, A.S.; Stolbov, D.N.; Maksimov, S.V.; Maslakov, K.I.; Chernavskii, P.A.; Pokusaeva, Y.A.; Koklin, A.E.; Bogdan, V.I.; Savilov, S.V. Sintered Fe/CNT framework catalysts for CO_2 hydrogenation into hydrocarbons. *Carbon* **2020**, *168*, 475–484. [CrossRef]
67. Williamson, D.L.; Herdes, C.; Torrente-Murciano, L.; Jones, M.D.; Mattia, D. N-Doped Fe@CNT for Combined RWGS/FT CO_2 Hydrogenation. *ACS Sustain. Chem. Eng.* **2019**, *7*, 7395–7402. [CrossRef]
68. Hwang, S.-M.; Zhang, C.; Han, S.J.; Park, H.-G.; Kim, Y.T.; Yang, S.; Jun, K.-W.; Kim, S.K. Mesoporous carbon as an effective support for Fe catalyst for CO_2 hydrogenation to liquid hydrocarbons. *J. CO2 Util.* **2020**, *37*, 65–73. [CrossRef]
69. Wei, J.; Ge, Q.; Yao, R.; Wen, Z.; Fang, C.; Guo, L.; Xu, H.; Sun, J. Directly converting CO_2 into a gasoline fuel. *Nat. Commun.* **2017**, *8*, 15174. [CrossRef]
70. Noreen, A.; Li, M.; Fu, Y.; Amoo, C.C.; Wang, J.; Maturura, E.; Du, C.; Yang, R.; Xing, C.; Sun, J. One-Pass Hydrogenation of CO_2 to Multibranched Isoparaffins over Bifunctional Zeolite-Based Catalysts. *ACS Catal.* **2020**, *10*, 14186–14194. [CrossRef]
71. Guo, L.; Sun, S.; Li, J.; Gao, W.; Zhao, H.; Zhang, B.; He, Y.; Zhang, P.; Yang, G.; Tsubaki, N. Boosting liquid hydrocarbons selectivity from CO_2 hydrogenation by facilely tailoring surface acid properties of zeolite via a modified Fischer-Tropsch synthesis. *Fuel* **2021**, *306*, 121684. [CrossRef]
72. Amoyal, M.; Vidruk-Nehemya, R.; Landau, M.V.; Herskowitz, M. Effect of potassium on the active phases of Fe catalysts for carbon dioxide conversion to liquid fuels through hydrogenation. *J. Catal.* **2017**, *348*, 29–39. [CrossRef]
73. Wei, J.; Sun, J.; Wen, Z.; Fang, C.; Ge, Q.; Xu, H. New insights into the effect of sodium on Fe_3O_4- based nanocatalysts for CO_2 hydrogenation to light olefins. *Catal. Sci. Technol.* **2016**, *6*, 4786–4793. [CrossRef]
74. Visconti, C.G.; Martinelli, M.; Falbo, L.; Infantes-Molina, A.; Lietti, L.; Forzatti, P.; Iaquaniello, G.; Palo, E.; Picutti, B.; Brignoli, F. CO_2 hydrogenation to lower olefins on a high surface area K-promoted bulk Fe-catalyst. *Appl. Catal. B Environ.* **2017**, *200*, 530–542. [CrossRef]
75. Boreriboon, N.; Jiang, X.; Song, C.; Prasassarakich, P. Fe-based bimetallic catalysts supported on TiO_2 for selective CO_2 hydrogenation to hydrocarbons. *J. CO2 Util.* **2018**, *25*, 330–337. [CrossRef]
76. Dry, M.E.; Shingles, T.; Boshoff, L.J.; Oosthuizen, G.J. Heats of chemisorption on promoted iron surfaces and the role of alkali in Fischer-Tropsch synthesis. *J. Catal.* **1969**, *15*, 190–199. [CrossRef]
77. Douglass, G.; Miller, M.M. A study of the effects of potassium addition to supported iron catalysts in the Fischer-Tropsch reaction. *J. Phys. Chem. B* **1988**, *92*, 6081–6085.
78. Bukur, D.B.; Mukesh, D.; Patel, S.A. Promoter effects on precipitated iron catalysts for Fischer-Tropsch synthesis. *Ind. Eng. Chem. Res.* **1990**, *29*, 194–204. [CrossRef]
79. Al-Dossary, M.; Ismail, A.A.; Fierro, J.L.G.; Bouzid, H.; Al-Sayari, S.A. Effect of Mn loading onto MnFeO nanocomposites for the CO_2 hydrogenation reaction. *Appl. Catal. B Environ.* **2015**, *165*, 651–660. [CrossRef]
80. Galvis, H.M.T.; Koeken, A.C.; Bitter, J.H.; Davidian, T.; Ruitenbeek, M.; Dugulan, A.I.; de Jong, K.P. Effects of sodium and sulfur on catalytic performance of supported iron catalysts for the Fischer–Tropsch synthesis of lower olefins. *J. Catal.* **2013**, *303*, 22–30. [CrossRef]
81. Yang, Y.; Xiang, H.-W.; Xu, Y.-Y.; Bai, L.; Li, Y.-W. Effect of potassium promoter on precipitated iron-manganese catalyst for Fischer–Tropsch synthesis. *Appl. Catal. A Gen.* **2004**, *266*, 181–194. [CrossRef]
82. Dai, L.; Chen, Y.; Liu, R.; Li, X.; Ullah, N.; Li, Z. CO_2 hydrogenation to C_{5+} hydrocarbons over K-promoted Fe/CNT catalyst: Effect of potassium on structure–activity relationship. *Appl. Organomet. Chem.* **2021**, *35*, e6253. [CrossRef]
83. Falbo, L.; Martinelli, M.; Visconti, C.G.; Lietti, L.; Forzatti, P.; Bassano, C.; Deiana, P. Effects of Zn and Mn Promotion in Fe-Based Catalysts Used for CO_x Hydrogenation to Long-Chain Hydrocarbons. *Ind. Eng. Chem. Res.* **2017**, *56*, 13147–13157. [CrossRef]
84. Guo, L.; Li, J.; Zeng, Y.; Kosol, R.; Cui, Y.; Kodama, N.; Guo, X.; Prasert, R.; Tharapong, V.; Liu, G.; et al. Heteroatom doped iron-based catalysts prepared by urea self-combustion method for efficient CO_2 hydrogenation. *Fuel* **2020**, *276*, 118102. [CrossRef]
85. Numpilai, T.; Chanlek, N.; Poo-Arporn, Y.; Cheng, C.K.; Siri-Nguan, N.; Sornchamni, T.; Chareonpanich, M.; Kongkachuichay, P.; Yigit, N.; Rupprechter, G.; et al. Tuning Interactions of Surface-adsorbed Species over $Fe-Co/K-Al_2O_3$ Catalyst by Different K Contents: Selective CO_2 Hydrogenation to Light Olefins. *ChemCatChem* **2020**, *12*, 3306–3320. [CrossRef]
86. Gong, W.; Ye, R.-P.; Ding, J.; Wang, T.; Shi, X.; Russell, C.K.; Tang, J.; Eddings, E.G.; Zhang, Y.; Fan, M. Effect of copper on highly effective Fe-Mn based catalysts during production of light olefins via Fischer-Tropsch process with low CO_2 emission. *Appl. Catal. B Environ.* **2020**, *278*, 119302. [CrossRef]
87. Velu, S.; Gangwal, S.K. Synthesis of alumina supported nickel nanoparticle catalysts and evaluation of nickel metal dispersions by temperature programmed desorption. *Solid State Ion.* **2006**, *177*, 803–811. [CrossRef]

88. Smeds, S.; Salmi, T.; Lindfors, L.P.; Krause, O. Chemisorption and TPD studies of hydrogen on Ni/Al_2O_3. *Appl. Catal. A Gen.* **1996**, *144*, 177–194. [CrossRef]
89. Willauer, H.D.; Ananth, R.; Olsen, M.T.; Drab, D.M.; Hardy, D.R.; Williams, F.W. Modeling and kinetic analysis of CO_2 hydrogenation using a Mn and K-promoted Fe catalyst in a fixed-bed reactor. *J. CO2 Util.* **2013**, *3–4*, 56–64. [CrossRef]
90. Ding, F.; Zhang, A.; Liu, M.; Zuo, Y.; Li, K.; Guo, X.; Song, C. CO_2 Hydrogenation to Hydrocarbons over Iron-based Catalyst: Effects of Physicochemical Properties of Al_2O_3 Supports. *Ind. Eng. Chem. Res.* **2014**, *53*, 17563–17569. [CrossRef]
91. Shi, Y.; Hou, S.; Qiu, X.; Zhao, B. MOFs-Based Catalysts Supported Chemical Conversion of CO_2. In *Metal-Organic Framework*; Springer: Cham, Switzerland, 2020; pp. 373–426.
92. Cui, W.G.; Zhang, G.Y.; Hu, T.L.; Bu, X.H. Metal-organic framework-based heterogeneous catalysts for the conversion of C1 chemistry: CO, CO_2 and CH_4. *Coord. Chem. Rev.* **2019**, *387*, 79–120. [CrossRef]
93. González-Cortés, S.L.; Imbert, F.E. Fundamentals, properties and applications of solid catalysts prepared by solution combustion synthesis (SCS). *Appl. Catal. A Gen.* **2013**, *452*, 117–131. [CrossRef]
94. Purohit, R.D.; Sharma, B.P.; Pillai, K.T.; Tyagi, A.K. Ultrafine ceria powders via glycine-nitrate combustion. *Mater. Res. Bull.* **2001**, *36*, 2711–2721. [CrossRef]
95. Dai, C.; Zhao, X.; Hu, B.; Zhang, J.; Hao, Q.; Chen, H.; Guo, X.; Ma, X. Hydrogenation of CO_2 to Aromatics over Fe–K/Alkaline Al_2O_3 and P/ZSM-5 Tandem Catalysts. *Ind. Eng. Chem. Res.* **2020**, *59*, 19194–19202. [CrossRef]
96. Liang, J.; Guo, L.; Gao, W.; Wang, C.; Guo, X.; He, Y.; Yang, G.; Tsubaki, N. Direct Conversion of CO_2 to Aromatics over K–Zn–Fe/ZSM-5 Catalysts via a Fischer–Tropsch Synthesis Pathway. *Ind. Eng. Chem. Res.* **2022**, *61*, 10336–10346. [CrossRef]
97. Abelló, S.; Montané, D. Exploring Iron-based Multifunctional Catalysts for Fischer–Tropsch Synthesis: A Review. *ChemSusChem* **2011**, *4*, 1538–1556. [CrossRef]
98. Chen, J.; Liang, T.; Li, J.; Wang, S.; Qin, Z.; Wang, P.; Huang, L.; Fan, W.; Wang, J. Regulation of Framework Aluminum Siting and Acid Distribution in H-MCM-22 by Boron Incorporation and Its Effect on the Catalytic Performance in Methanol to Hydrocarbons. *ACS Catal.* **2016**, *6*, 2299–2313. [CrossRef]
99. Bjørgen, M.; Akyalcin, S.; Olsbye, U.; Benard, S.; Kolboe, S.; Svelle, S. Methanol to hydrocarbons over large cavity zeolites: Toward a unified description of catalyst deactivation and the reaction mechanism. *J. Catal.* **2010**, *275*, 170–180. [CrossRef]
100. Wei, J.; Yao, R.; Ge, Q.; Wen, Z.; Ji, X.; Fang, C.; Zhang, J.; Xu, H.; Sun, J. Catalytic Hydrogenation of CO_2 to Isoparaffins over Fe-Based Multifunctional Catalysts. *ACS Catal.* **2018**, *8*, 9958–9967. [CrossRef]
101. Su, X.; Yang, X.; Zhao, B.; Huang, Y. Designing of highly selective and high-temperature endurable RWGS heterogeneous catalysts: Recent advances and the future directions. *J. Energy Chem.* **2017**, *26*, 854–867. [CrossRef]
102. Maitlis, P.M.; Zanotti, V. The role of electrophilic species in the Fischer–Tropsch reaction. *Chem. Commun.* **2009**, *13*, 1619–1634. [CrossRef]
103. Dry, M.E. The Fischer–Tropsch process: 1950–2000. *Catal. Today* **2002**, *71*, 227–241. [CrossRef]
104. Xu, Y.; Shi, C.; Liu, B.; Wang, T.; Zheng, J.; Li, W.; Liu, D.; Liu, X. Selective production of aromatics from CO_2. *Catal. Sci. Technol.* **2019**, *9*, 593–610. [CrossRef]
105. Jiang, J.; Wen, C.; Tian, Z.; Wang, Y.; Zhai, Y.; Chen, L.; Li, Y.; Liu, Q.; Wang, C.; Ma, L. Manganese-Promoted Fe_3O_4 Microsphere for Efficient Conversion of CO_2 to Light Olefins. *Ind. Eng. Chem. Res.* **2020**, *59*, 2155–2162. [CrossRef]
106. Ramirez, A.; Gevers, L.; Bavykina, A.; Ould-Chikh, S.; Gascon, J. Metal Organic Framework-Derived Iron Catalysts for the Direct Hydrogenation of CO_2 to Short Chain Olefins. *ACS Catal.* **2018**, *8*, 9174–9182. [CrossRef]
107. Lyons, T.W.; Guironnet, D.; Findlater, M.; Brookhart, M. Synthesis of p-Xylene from Ethylene. *J. Am. Chem. Soc.* **2012**, *134*, 15708–15711. [CrossRef]
108. Shen, X.Q.; Kang, J.C.; Niu, W.; Wang, M.H.; Zhang, Q.H.; Wang, Y. Impact of hierarchical pore structure on the catalytic performances of MFI zeolites modified by ZnO for the conversion of methanol to aromatics. *Catal. Sci. Technol.* **2017**, *7*, 3598–3612. [CrossRef]
109. Niziolek, A.M.; Onel, O.; Floudas, C.A. Production of benzene, toluene, and xylenes from natural gas via methanol: Process synthesis and global optimization. *AIChE J.* **2016**, *62*, 1531–1556. [CrossRef]
110. Yang, X.; Su, X.; Chen, D.; Zhang, T.; Huang, Y. Direct conversion of syngas to aromatics: A review of recent studies. *Chin. J. Catal.* **2020**, *41*, 561–573. [CrossRef]
111. Wen, C.; Jiang, J.; Cai, C.; Tian, Z.; Xu, X.; Wu, J.; Wang, C.; Ma, L. Single-Step Selective Conversion of Carbon Dioxide to Aromatics over Na-Fe_3O_4/Hierarchical HZSM-5 Zeolite Catalyst. *Energy Fuels* **2020**, *34*, 11282–11289. [CrossRef]
112. Wang, S.W.; Wu, T.J.; Lin, J.; Tian, J.; Ji, Y.S.; Pei, Y.; Yan, S.R.; Qiao, M.H.; Xu, H.L.; Zong, B.N. FeK on 3D Graphene-Zeolite Tandem Catalyst with High Efficiency and Versatility in Direct CO_2 Conversion to Aromatics. *ACS Sustain. Chem. Eng.* **2019**, *7*, 17825–17833. [CrossRef]
113. Wang, Y.; Kazumi, S.; Gao, W.; Gao, X.; Li, H.; Guo, X.; Yoneyama, Y.; Yang, G.; Tsubaki, N. Direct conversion of CO_2 to aromatics with high yield via a modified Fischer-Tropsch synthesis pathway. *Appl. Catal. B Environ.* **2020**, *269*, 118792. [CrossRef]
114. Wei, J.; Yao, R.; Ge, Q.; Xu, D.; Fang, C.; Zhang, J.; Xu, H.; Sun, J. Precisely regulating Brønsted acid sites to promote the synthesis of light aromatics via CO_2 hydrogenation. *Appl. Catal. B Environ.* **2021**, *283*, 119648. [CrossRef]
115. Song, G.; Li, M.; Yan, P.; Nawaz, M.A.; Liu, D. High Conversion to Aromatics via CO_2-FT over a CO-Reduced Cu-Fe_2O_3 Catalyst Integrated with HZSM-5. *ACS Catal.* **2020**, *10*, 11268–11279. [CrossRef]

116. Sibi, M.G.; Khan, M.K.; Verma, D.; Yoon, W.; Kim, J. High-yield synthesis of BTEX over Na-FeAlO$_x$/Zn-HZSM-5@SiO$_2$ by direct CO$_2$ conversion and identification of surface intermediates. *Appl. Catal. B Environ.* **2022**, *301*, 120813. [CrossRef]
117. Gao, W.; Guo, L.; Wu, Q.; Wang, C.; Guo, X.; He, Y.; Zhang, P.; Yang, G.; Liu, G.; Wu, J.; et al. Capsule-like zeolite catalyst fabricated by solvent-free strategy for para-Xylene formation from CO$_2$ hydrogenation. *Appl. Catal. B Environ.* **2022**, *303*, 120906. [CrossRef]
118. Ramirez, A.; Chowdhury, A.D.; Dokania, A.; Cnudde, P.; Caglapn, M.; Yarulina, I.; Abou-Hamad, E.; Gevers, L.; Ould-Chikh, S.; De Wispelaere, K.; et al. Effect of Zeolite Topology and Reactor Configuration on the Direct Conversion of CO$_2$ to Light Olefins and Aromatics. *ACS Catal.* **2019**, *9*, 6320–6334. [CrossRef]
119. Wang, D.; Xie, Z.; Porosoff, M.D.; Chen, J.G. Recent advances in carbon dioxide hydrogenation to produce olefins and aromatics. *Chem* **2021**, *7*, 2277–2311. [CrossRef]
120. Ra, E.C.; Kim, K.Y.; Kim, E.H.; Lee, H.; An, K.; Lee, J.S. Recycling Carbon Dioxide through Catalytic Hydrogenation: Recent Key Developments and Perspectives. *ACS Catal.* **2020**, *10*, 11318–11345. [CrossRef]
121. Hong, S.Y.; Dong, H.C.; Yang, J.I.; Jung, H.; Ji, C.P. A new synthesis of carbon encapsulated Fe$_5$C$_2$ nanoparticles for high-temperature Fischer–Tropsch synthesis. *Nanoscale* **2015**, *7*, 16616–16620. [CrossRef]
122. You, Z.; Deng, W.; Zhang, Q.; Wang, Y. Hydrogenation of carbon dioxide to light olefins over non-supported iron catalyst. *Chin. J. Catal.* **2013**, *34*, 956–963. [CrossRef]
123. Ngantsoue-Hoc, W.; Zhang, Y.; O'Brien, R.J.; Luo, M.; Davis, B.H. Fischer−Tropsch synthesis: Activity and selectivity for Group I alkali promoted iron-based catalysts. *Appl. Catal. A Gen.* **2002**, *236*, 77–89. [CrossRef]
124. Rongxian, B.; Yisheng, T.; Yizhuo, H. Study on the carbon dioxide hydrogenation to iso-alkanes over Fe–Zn–M/zeolite composite catalysts. *Fuel Processing Technol.* **2004**, *86*, 293–301. [CrossRef]
125. Wu, T.J.; Lin, J.; Cheng, Y.; Tian, J.; Wang, S.W.; Xie, S.H.; Pei, Y.; Yan, S.R.; Qiao, M.H.; Xu, H.L.; et al. Porous Graphene-Confined Fe-K as Highly Efficient Catalyst for CO$_2$ Direct Hydrogenation to Light Olefins. *ACS Appl. Mater. Inter.* **2018**, *10*, 23439–23443. [CrossRef] [PubMed]
126. Wang, H.; Sun, K.; Tao, F.; Stacchiola, D.J.; Hu, Y.H. 3D Honeycomb-Like Structured Graphene and Its High Efficiency as a Counter-Electrode Catalyst for Dye-Sensitized Solar Cells. *Angew. Chem. Int. Ed.* **2013**, *52*, 9210–9214. [CrossRef] [PubMed]
127. Zhang, J.; Zhang, M.; Chen, S.; Wang, X.; Zhou, Z.; Wu, Y.; Zhang, T.; Yang, G.; Han, Y.; Tan, Y. Hydrogenation of CO$_2$ into aromatics over a ZnCrO$_x$-zeolite composite catalyst. *Chem. Commun.* **2019**, *55*, 973–976. [CrossRef]
128. Xu, Y.; Liu, D.; Liu, X. Conversion of syngas toward aromatics over hybrid Fe-based Fischer-Tropsch catalysts and HZSM-5 zeolites. *Appl. Catal. A Gen.* **2018**, *552*, 168–183. [CrossRef]
129. Jia, Y.; Wang, J.; Zhang, K.; Chen, G.; Yang, Y.; Liu, S.; Ding, C.; Meng, Y.; Liu, P. Hierarchical ZSM-5 zeolite synthesized via dry gel conversion-steam assisted crystallization process and its application in aromatization of methanol. *Powder Technol.* **2018**, *328*, 415–429. [CrossRef]
130. Hirota, Y.; Murata, K.; Tanaka, S.; Nishiyama, N.; Egashira, Y.; Ueyama, K. Dry gel conversion synthesis of SAPO-34 nanocrystals. *Mater. Chem. Phys.* **2010**, *123*, 507–509. [CrossRef]
131. Meng, Y.; Genuino, H.C.; Kuo, C.-H.; Huang, H.; Chen, S.-Y.; Zhang, L.; Rossi, A.; Suib, S.L. One-Step Hydrothermal Synthesis of Manganese-Containing MFI-Type Zeolite, Mn–ZSM-5, Characterization, and Catalytic Oxidation of Hydrocarbons. *J. Am. Chem. Soc.* **2013**, *135*, 8594–8605. [CrossRef]
132. Jia, Y.; Wang, J.; Zhang, K.; Feng, W.; Liu, S.; Ding, C.; Liu, P. Nanocrystallite self-assembled hierarchical ZSM-5 zeolite microsphere for methanol to aromatics. *Microporous Mesoporous Mater.* **2017**, *247*, 103–115. [CrossRef]
133. Schwieger, W.; Machoke, A.G.; Weissenberger, T.; Inayat, A.; Selvam, T.; Klumpp, M.; Inayat, A. Hierarchy concepts: Classification and preparation strategies for zeolite containing materials with hierarchical porosity. *Chem. Soc. Rev.* **2016**, *45*, 3353–3376. [CrossRef] [PubMed]
134. Wang, Y.; Wu, W.; Rao, Y.; Li, Z.; Tsubaki, N.; Wu, M. Cation modulating electrocatalyst derived from bimetallic metal–organic frameworks for overall water splitting. *J. Mater. Chem. A* **2017**, *5*, 6170–6177. [CrossRef]
135. Zhang, C.; Kwak, G.; Park, H.-G.; Jun, K.-W.; Lee, Y.-J.; Kang, S.C.; Kim, S. Light hydrocarbons to BTEX aromatics over hierarchical HZSM-5: Effects of alkali treatment on catalytic performance. *Microporous Mesoporous Mater.* **2019**, *276*, 292–301. [CrossRef]
136. Zhang, C.; Kwak, G.; Lee, Y.-J.; Jun, K.-W.; Gao, R.; Park, H.-G.; Kim, S.; Min, J.-E.; Kang, S.C.; Guan, G. Light hydrocarbons to BTEX aromatics over Zn-modified hierarchical ZSM-5 combined with enhanced catalytic activity and stability. *Microporous Mesoporous Mater.* **2019**, *284*, 316–326. [CrossRef]
137. Stepanov, A.G.; Arzumanov, S.S.; Gabrienko, A.A.; Parmon, V.N.; Ivanova, I.I.; Freude, D. Significant influence of Zn on activation of the C-H bonds of small alkanes by Bronsted acid sites of zeolite. *Chemphyschem* **2008**, *9*, 2559–2563. [CrossRef] [PubMed]
138. Zhao, X.; Chu, Y.; Qi, G.; Wang, Q.; Gao, W.; Wang, X.; Li, S.; Xu, J.; Deng, F. Probing the active sites for methane activation on Ga/ZSM-5 zeolites with solid-state NMR spectroscopy. *Chem. Commun.* **2020**, *56*, 12029–12032. [CrossRef]
139. Schreiber, M.W.; Plaisance, C.P.; Baumgärtl, M.; Reuter, K.; Jentys, A.; Bermejo-Deval, R.; Lercher, J.A. Lewis–Brønsted Acid Pairs in Ga/H-ZSM-5 To Catalyze Dehydrogenation of Light Alkanes. *J. Am. Chem. Soc.* **2018**, *140*, 4849–4859. [CrossRef]
140. Uslamin, E.A.; Saito, H.; Sekine, Y.; Hensen, E.J.M.; Kosinov, N. Different mechanisms of ethane aromatization over Mo/ZSM-5 and Ga/ZSM-5 catalysts. *Catal. Today* **2021**, *369*, 184–192. [CrossRef]
141. Zhang, J.; Qian, W.; Kong, C.; Wei, F. Increasing para-Xylene Selectivity in Making Aromatics from Methanol with a Surface-Modified Zn/P/ZSM-5 Catalyst. *ACS Catal.* **2015**, *5*, 2982–2988. [CrossRef]

142. Miao, D.; Ding, Y.; Yu, T.; Li, J.; Pan, X.; Bao, X. Selective Synthesis of Benzene, Toluene, and Xylenes from Syngas. *ACS Catal.* **2020**, *10*, 7389–7397. [CrossRef]
143. Baertsch, C.D.; Funke, H.H.; Falconer, J.L.; Noble, R.D. Permeation of Aromatic Hydrocarbon Vapors through Silicalite−Zeolite Membranes. *J. Phys. Chem.* **1996**, *100*, 7676–7679. [CrossRef]
144. Zheng, S.; Heydenrych, H.R.; Jentys, A.; Lercher, J.A. Influence of Surface Modification on the Acid Site Distribution of HZSM-5. *J. Phys. Chem. B* **2002**, *106*, 9552–9558. [CrossRef]
145. Gao, J.J.; Wang, Y.L.; Ping, Y.; Hu, D.C.; Xu, G.W.; Gu, F.N.; Su, F.B. A thermodynamic analysis of methanation reactions of carbon oxides for the production of synthetic natural gas. *RSC Adv.* **2012**, *2*, 2358–2368. [CrossRef]
146. Moon, S.; Chae, H.-J.; Park, M.B. Oligomerization of light olefins over ZSM-5 and beta zeolite catalysts by modifying textural properties. *Appl. Catal. A Gen.* **2018**, *553*, 15–23. [CrossRef]
147. Li, Z.; Qu, Y.; Wang, J.; Liu, H.; Li, M.; Miao, S.; Li, C. Highly Selective Conversion of Carbon Dioxide to Aromatics over Tandem Catalysts. *Joule* **2019**, *3*, 570–583. [CrossRef]
148. Zecevic, J.; Vanbutsele, G.; de Jong, K.P.; Martens, J.A. Nanoscale intimacy in bifunctional catalysts for selective conversion of hydrocarbons. *Nature* **2015**, *528*, 245–248. [CrossRef]
149. Cheng, K.; Gu, B.; Liu, X.L.; Kang, J.C.; Zhang, Q.H.; Wang, Y. Direct and Highly Selective Conversion of Synthesis Gas into Lower Olefins: Design of a Bifunctional Catalyst Combining Methanol Synthesis and Carbon-Carbon Coupling. *Angew. Chem.* **2016**, *128*, 4803–4806. [CrossRef]
150. Li, M.Z.; Nawaz, M.A.; Song, G.Y.; Zaman, W.Q.; Liu, D.H. Influential Role of Elemental Migration in a Composite Iron-Zeolite Catalyst for the Synthesis of Aromatics from Syngas. *Ind. Eng. Chem. Res.* **2020**, *59*, 9043–9054. [CrossRef]
151. Su, T.; Qin, Z.; Huang, G.; Ji, H.; Jiang, Y.; Chen, J. Density functional theory study on the interaction of CO_2 with Fe_3O_4(111) surface. *Appl. Surf. Sci.* **2016**, *378*, 270–276. [CrossRef]
152. Hakim, A.; Marliza, T.S.; Abu Tahari, N.M.; Wan Isahak, R.W.N.; Yusop, R.M.; Mohamed Hisham, W.M.; Yarmo, A.M. Studies on CO_2 Adsorption and Desorption Properties from Various Types of Iron Oxides (FeO, Fe_2O_3, and Fe_3O_4). *Ind. Eng. Chem. Res.* **2016**, *55*, 7888–7897. [CrossRef]
153. Kattel, S.P.; Liu, P.; Chen, J. Tuning Selectivity of CO_2 Hydrogenation Reactions at the Metal/Oxide Interface. *J. Am. Chem. Soc.* **2017**, *139*, 9739–9754. [CrossRef]
154. Pham, T.H.; Qi, Y.; Yang, J.; Duan, X.; Qian, G.; Zhou, X.; Chen, D.; Yuan, W. Insights into Hägg Iron-Carbide-Catalyzed Fischer–Tropsch Synthesis: Suppression of CH_4 Formation and Enhancement of C–C Coupling on χ-Fe_5C_2 (510). *ACS Catal.* **2015**, *5*, 2203–2208. [CrossRef]
155. Ye, R.P.; Ding, J.; Gong, W.B.; Argyle, M.D.; Zhong, Q.; Wang, Y.J.; Russell, C.K.; Xu, Z.H.; Russell, A.G.; Li, Q.H.; et al. CO_2 hydrogenation to high-value products via heterogeneous catalysis. *Nat. Commun.* **2019**, *10*, 5698. [CrossRef] [PubMed]
156. Pham, T.H.; Duan, X.; Qian, G.; Zhou, X.; Chen, D. CO Activation Pathways of Fischer–Tropsch Synthesis on χ-Fe_5C_2 (510): Direct versus Hydrogen-Assisted CO Dissociation. *J. Phys. Chem. C* **2014**, *118*, 10170–10176. [CrossRef]
157. Nie, X.; Wang, H.; Janik, M.J.; Chen, Y.; Guo, X.; Song, C. Mechanistic Insight into C–C Coupling over Fe–Cu Bimetallic Catalysts in CO_2 Hydrogenation. *J. Phys. Chem. C* **2017**, *121*, 13164–13174. [CrossRef]
158. van Santen, R.A.; Markvoort, A.J.; Filot, I.A.W.; Ghouri, M.M.; Hensen, E.J.M. Mechanism and microkinetics of the Fischer-Tropsch reaction. *Phys. Chem. Chem. Phys.* **2013**, *15*, 17038–17063. [CrossRef]
159. Helden, P.V.; Berg, J.A.V.D.; Petersen, M.A.; Rensburg, W.J.V.; Ciobc, I.M.; Loosdrecht, J.V.D. Computational investigation of the kinetics and mechanism of the initial steps of the Fischer–Tropsch synthesis on cobalt. *Faraday Discuss.* **2017**, *197*, 117–151. [CrossRef]
160. Yao, Z.; Guo, C.; Mao, Y.; Hu, P. Quantitative Determination of C–C Coupling Mechanisms and Detailed Analyses on the Activity and Selectivity for Fischer–Tropsch Synthesis on Co(0001): Microkinetic Modeling with Coverage Effects. *ACS Catal.* **2019**, *9*, 5957–5973. [CrossRef]
161. Qi, Y.; Yang, J.; Holmen, A.; Chen, D. Investigation of $C_1 + C_1$ Coupling Reactions in Cobalt-Catalyzed Fischer-Tropsch Synthesis by a Combined DFT and Kinetic Isotope Study. *Catalysts* **2019**, *9*, 551. [CrossRef]
162. Asiaee, A.; Benjamin, K.M. A density functional theory based elementary reaction mechanism for early steps of Fischer-Tropsch synthesis over cobalt catalyst. 1. Reaction kinetics. *Mol. Catal.* **2017**, *436*, 218–227. [CrossRef]
163. Wang, B.; Liang, D.; Zhang, R.; Ling, L. Crystal Facet Dependence for the Selectivity of C2 Species over Co2C Catalysts in the Fischer–Tropsch Synthesis. *J. Phys. Chem. C* **2018**, *122*, 29249–29258. [CrossRef]
164. Liu, H.X.; Zhang, R.G.; Ling, L.X.; Wang, Q.; Wang, B.J.; Li, D.B. Insight into the preferred formation mechanism of long-chain hydrocarbons in Fischer-Tropsch synthesis on Hcp Co(10–11) surfaces from DFT and microkinetic modeling. *Catal. Sci. Technol.* **2017**, *7*, 3758–3776. [CrossRef]
165. Batchu, R.; Galvita, V.V.; Alexopoulos, K.; Van der Borght, K.; Poelman, H.; Reyniers, M.-F.; Marin, G.B. Role of intermediates in reaction pathways from ethene to hydrocarbons over H-ZSM-5. *Appl. Catal. A Gen.* **2017**, *538*, 207–220. [CrossRef]
166. Wang, X.; Shen, M.; Song, L.; Su, Y.; Wang, J. Surface basicity on bulk modified phosphorus alumina through different synthesis methods. *Phys. Chem. Chem. Phys.* **2011**, *13*, 15589–15596. [CrossRef]
167. Busca, G.; Lorenzelli, V. Infrared spectroscopic identification of species arising from reactive adsorption of carbon oxides on metal oxide surfaces. *J. Mater. Chem.* **1982**, *7*, 89–126. [CrossRef]

168. Turek, A.M.; Wachs, I.E.; DeCanio, E. Acidic properties of alumina-supported metal oxide catalysts: An infrared spectroscopy study. *J. Phys. Chem.* **1992**, *96*, 5000–5007. [CrossRef]
169. Ilias, S.; Bhan, A. Mechanism of the Catalytic Conversion of Methanol to Hydrocarbons. *ACS Catal.* **2013**, *3*, 18–31. [CrossRef]
170. Cheng, K.; Zhou, W.; Kang, J.; He, S.; Shi, S.; Zhang, Q.; Pan, Y.; Wen, W.; Wang, Y. Bifunctional Catalysts for One-Step Conversion of Syngas into Aromatics with Excellent Selectivity and Stability. *Chem* **2017**, *3*, 334–347. [CrossRef]
171. Tran, T.V.; Le-Phuc, N.; Nguyen, T.H.; Dang, T.T.; Ngo, P.T.; Nguyen, D.A. Application of NaA Membrane Reactor for Methanol Synthesis in CO_2 Hydrogenation at Low Pressure. *Int. J. Chem. React. Eng.* **2018**, *16*. [CrossRef]